



The United Nations
University

GEOTHERMAL TRAINING PROGRAMME
Orkustofnun, Grensasvegur 9,
IS-108 Reykjavik, Iceland

Reports 1994
Number 1

A CONCEPTUAL MODEL AND RESERVOIR ASSESSMENT FOR THE MUTNOVSKY GEOTHERMAL FIELD, KAMCHATKA, RUSSIA

Stephan Assaoulov
Kamchatka Heat & Power Co.,
19 Krasintseva st.,
683032, Petropavlovsk-Kamchatsky,
RUSSIA

ABSTRACT

In this report, a general description is given on the Mutnovsky geothermal field. Evaluation of formation temperature and well pressure data is presented. The results of these studies are incorporated into a conceptual model of the geothermal system. An upflow zone of $\geq 300^{\circ}\text{C}$ water is assumed underneath the Mutnovsky volcano, south of the wellfield. The fluid flows laterally towards the north into the present wellfield, where the flow changes direction towards the northeast. All the reservoir volume seems to be in a single-phase, liquid condition, apart from a steam zone in the central part of the wellfield.

Wellbore simulation studies indicate that during production the Mutnosky wells flash down to their feedzones and some distance into the reservoir. The enthalpy increases with time during production for wells producing from the single-phase liquid zone. A quantitative study of the production capacity, by using volumetric assessment and random distribution in some of the reservoir properties, suggests that up to 80 MW of electric power can be produced for a 30-year generation period.

1. INTRODUCTION

The Mutnovsky geothermal field is located in the southern part of Kamchatka peninsula in NE-Russia (Figure 1). The geothermal exploration of the field was carried out during 1978-1990. In the initial phase, geological and geophysical surveys were carried out from 1978-1983. Since 1983, more than 80 wells have been drilled covering an area of about 25 km². The depth of wells ranges from 1000 to 2500 m. The drilling identified prospect sites in the Mutnovsky area. These are referred to as the southern site, the central site and the northeastern site. Unfortunately, the accessibility of the southern site is poor due to rough terrain. A reservoir assessment that included only the central and the northeastern sites, estimated production capacities of 121 kg/s of steam for the central site and 35 kg/s of steam for the northeastern site of the reservoir.

At present there are plans to construct an 80 MW_e power plant in the central site. The Mutnovsky reservoir is liquid-dominated, therefore, additional plans are for using the separated liquid for a heating station to provide heated groundwater for district heating in the Petropavlovsk-Kamchatsky area.

The following report presents a reservoir evaluation study for the Mutnovsky field. It is a part of the 1994 UNU Geothermal Training Programme at Orkustofnun - National Energy Authority, Reykjavik, Iceland

during April to October 1994. An outline is given of the reservoir geology, an evaluation of reservoir pressure and formation temperature is made, and a conceptual reservoir model is presented. The conceptual model is, furthermore, used as a base for volumetric assessment study using the Monte-Carlo probability method.

2. GENERAL OUTLINE OF THE MUTNOVSKY GEOTHERMAL FIELD

2.1 Location and access

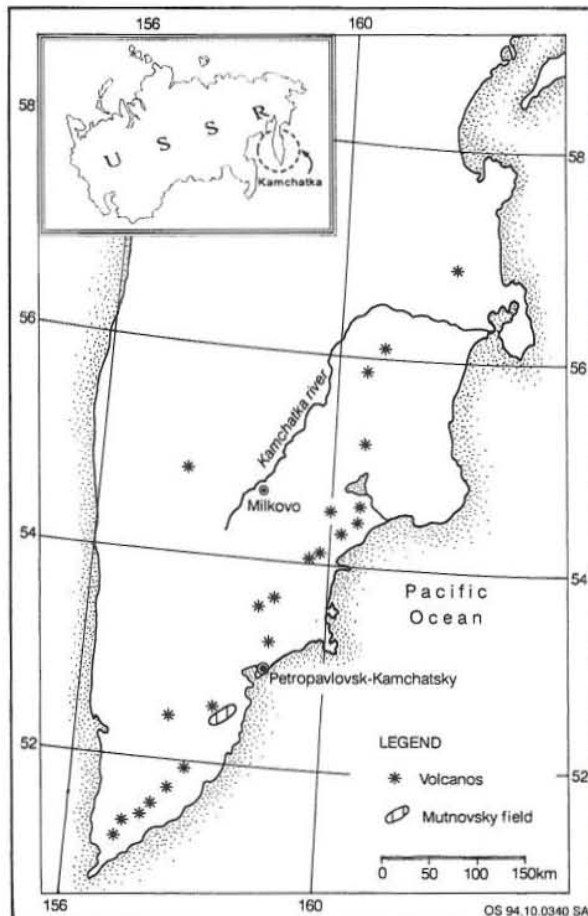


FIGURE 1: Location of the Mutnovsky geothermal field

The Mutnovsky geothermal field is located approximately 75 km south of the Petropavlovsk-Kamchatsky city in the Kamchatka peninsula, in the far eastern part of Russia (Figure 1). The Mutnovsky field belongs to the Southern Kamchatka volcanic zone, about 8 km to the north of the Mutnovsky volcano. The field is connected with the city of Petropavlovsk-Kamchatsky by a 125 km long road whereof the last 65 km are unpaved. The access to the field is very difficult during winter time because of heavy snowfalls, requiring snow removal for access.

2.2 Geology

From the morphological point of view, the Mutnovsky area is represented as a volcanic plateau at an elevation of 700-900 m a.s.l. that is dissected by the canyon valleys of the Mutnovskaja, Falshivaja and Zhirovaja rivers (Figure 2). There are several extrusive domes and slag cones on the plateau.

The Mutnovsky area is a region with very intensive volcanic activity. There are two active volcanoes - Mutnovsky and Gorely and one extinct and eroded volcano, Zhirovskoy, in the vicinity of the geothermal field. The Mutnovsky volcano is characterized by the most powerful fumaroles on the Kamchatka peninsula (Vakin et al., 1976).

The Mutnovsky geothermal system is confined to a graben depression among volcanos that is intersected by faults of three different strikes (Vakin et al., 1976). These are:

- a) The Paratunsko-Assachinskaja meridional fault zone;
- b) The Gorelovskaja latitudinal fault zone;
- c) The Mutnovskaja fault zone with NE-SW orientation.

The area is very complicated tectonically, due to its location on the boundaries between the southern Kamchatka's graben-syncline and the eastern gorst-anticlinorium. The stratigraphic sequence of the Mutnovsky field consists of volcanic rocks with age ranging from Oligocene (Pg_3) to Upper-Quaternary (Q_m).

Tuff and lava are represented by andesite-dacite, andesite and andesite-basalt. Intrusions and dykes have variable composition from diorite, dacite, andesite to basalt and geological age range from Miocene to Quaternary (Vakin et al., 1976).

The caprocks overlaying the Mutnovsky geothermal reservoir consist of Pliocene-Quaternary rocks with very variable thickness ranging from 200 to 1200 m. These rocks are assumed to be unpermeable except at several places along the Paratunsko-Avachinskaja meridional fault zone where they are intersected by faults allowing the geothermal fluid to rise to the surface (Figure 2).

The geothermal reservoir is mainly composed of Oligocene-Miocene rocks (Pg_3-N_1) which are hydrothermally altered and cracked. The width of cracks, as seen in cores, ranges from hairline to 25 mm with quartzitic and carbonaceous crack-filling. A prophyllitic face is presented in the geothermal reservoir with alteration temperatures of 200-300°C and is characterized by the presence of epidote. The thickness of Oligocene-Miocene rocks, as observed in wells, is about 2000 m.

2.3 Hydrogeology

One of the main features of the Mutnovsky geothermal field is a powerful thermal activity on the surface. Fumaroles, hot springs and thermal grounds are located along the Paratunsko-Assachinskaja meridional fault zone and range from the Mutnovsky volcano's crater to the valley of the Zhirovaja river, 20 km to the northnortheast (Figure 2). The estimated heat losses from springs decrease versus distance from the volcano. They have been estimated as 2000 MW_t in the crater, 60 MW_t in the Mutnovsky area and about 30 MW_t in the valley of Zhirovaja river (Vakin et al., 1976).

A shallow cold groundwater aquifer is only found in the northern part of the Mutnovsky area and is associated with a ground water flow from the caldera of the Gorely volcano in the west (the main recharge area)

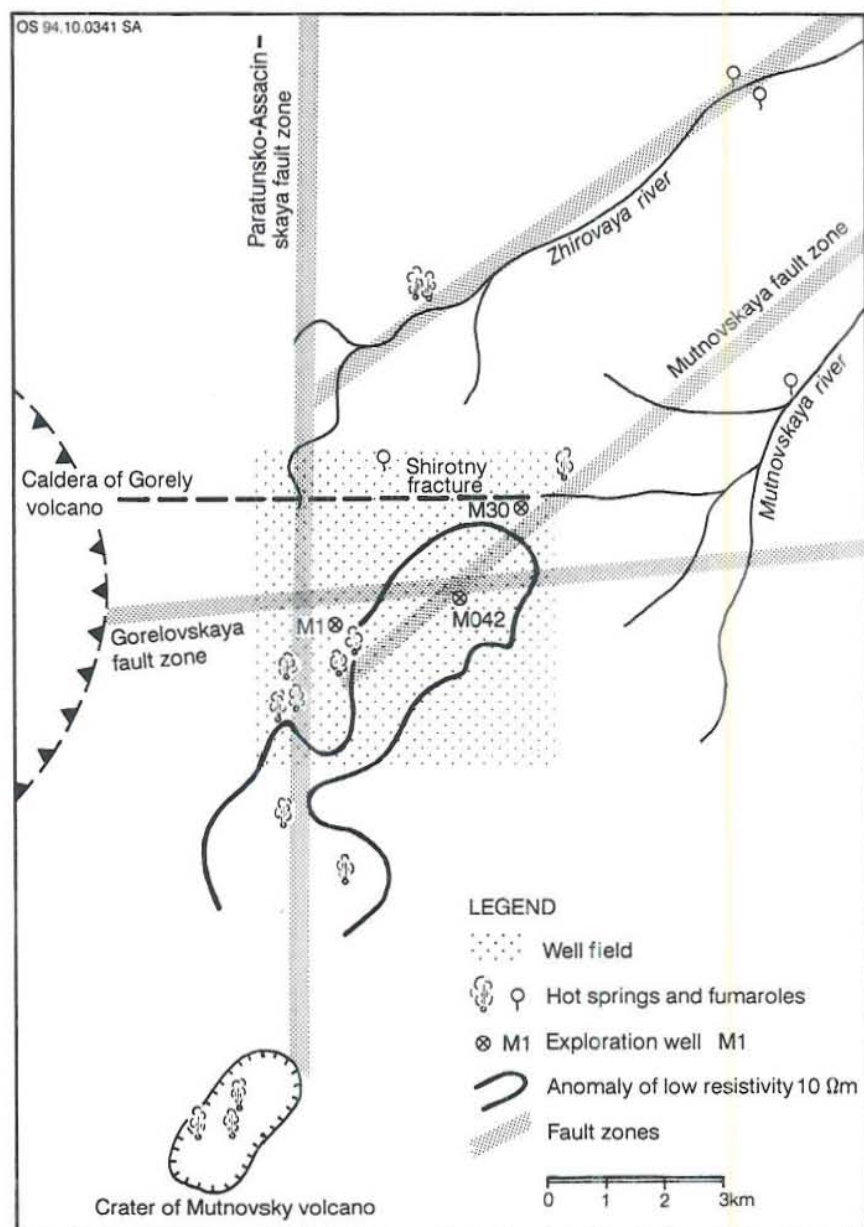


FIGURE 2: General overview of the Mutnovsky geothermal field

towards the Pacific ocean in the east. This shallow aquifer is mainly composed of Pliocene tuffs intersected by pyroclastic material. Its thickness is about 200 m. The average permeability is 10-20 D (D=Darcy) and the hydraulic gradient in the range 0.03-0.07 m/m. The total dissolved solids in the cold water is about 0.3 g/l and the water has a calcium-sodium carbonate composition (Perveev et al., 1992).

The host rock of the Mutnovsky geothermal reservoir is of Oligocene-Pliocene composition. The permeability of the rocks is predominantly secondary due to fractures and is, therefore, extremely anisotropic. The average permeability thickness, as measured in welltests is around 1 Dm. Fluid enters the wells (feed zones) at 500-2200 m depth except in well Mv-2 where the main feed zone is at about 250 m (Figure 3). The elevation of the static water level in the Mutnovsky reservoir decreases from the south (400 m a.s.l.) to the north (200 m a.s.l.) except in the central part of the wellfield where water level rises to 450 - 550 m a.s.l. The reservoir fluid is a low-gas, diluted sodium-chloride brine with total dissolved solids about 1.0-1.5 g/l. Noncondensable gases (manily CO₂ and N₂) in the steam reach about 0.14 weight percent. Carbon dioxide is the prevalent gas (50-95%).

2.4 Geophysical studies

The geothermal exploration in the Mutnovsky geothermal field has relied heavily on geophysical methods. The primary geophysical exploration tools employed were electrical resistivity and magnetotelluric surveys. An anomaly of low resistivity rocks outlines the primary target areas for a commercial geothermal reservoir at Mutnovsky. This anomaly is delineated by fractures striking north and northeast (Figure 2). The anomaly

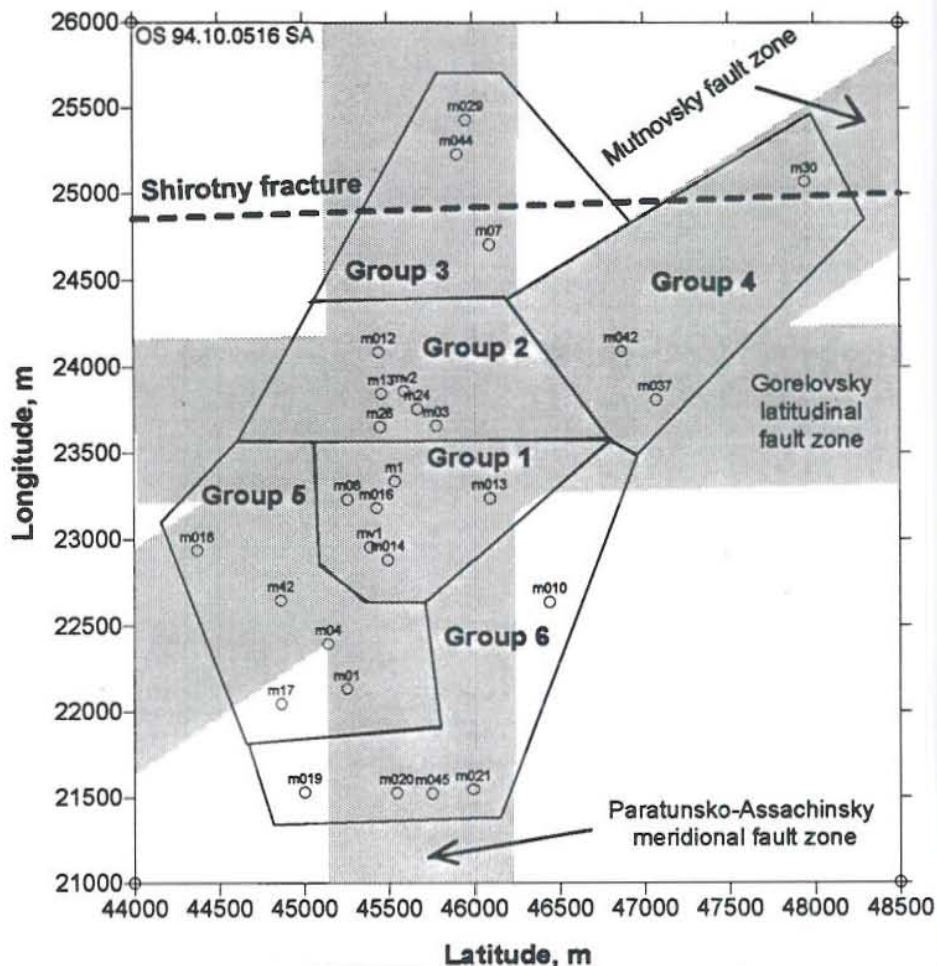


FIGURE 3: Location and grouping of wells in the Mutnovsky wellfield

extends from the slopes of the Mutnovsky volcano in the south along the Paratunsko-Assachinsky fault zone until the central site of the Mutnovsky geothermal field where the low resistivity anomaly changes direction to northeast, towards the old Zhirovsky volcano. There is a good correlation between the surface geothermal activity and the low resistivity anomaly in the Mutnovsky area (Perveev et al., 1992).

3. EVALUATION OF THE MUTNOVSKY GEOTHERMAL RESERVOIR

3.1 General information on wells

Geothermal drilling in the Mutnovsky area was initiated in 1978, when several shallow exploration wells were drilled. Two of them (Mv-1 and Mv-2) were successful producers. Exploitation drilling was started in 1983, using oil-well drill rigs for reaching well depth down to 1500-2500 m. Figure 3 shows the location of the wells in the Mutnovsky area and Table 1 records general information about the wells. The size of the Mutnovsky wellfield is approximately 7 km².

TABLE 1: An overview of wells in the Mutnovsky area

Well	Drill date		Location		Well design		Depth (m)	Elevation (m a.s.l.)	Status of well
	From	To	N-S (m)	E-W (m)	Casing 245 mm	Liner 168 mm			
Mv-1	78	79	22956	45394			555	784	Cemented
Mv-2	78	79	23858	45564			618	799	Cemented
M-1	04.79	09.80	23336	45540	804	---	1523	786	Productive
M-13	11.82	05.83	23843	45461			830	809	Monitoring
M-17	04.83	08.83	22042	44867			1300	793	Monitoring
M-24	09.83	01.84	23754	45673	1000	---	1300	793	Productive
M-26	01.84	05.84	23650	45455	---	0-466	466	816	Productive
M-30	06.84	10.84	25070	47950			1467	794	Monitoring
M-42	10.84	03.85	22646	44866			970	845	Monitoring
M-01	05.85	10.85	22131	45254	700	600-1195	1195	807	Productive
M-03	10.85	04.86	23657	45787			1486	786	Non-productive
M-04	04.86	07.86	22395	45146			2100	820	Non-productive
M-07	05.85	08.85	24704	46096			1503	804	Monitoring
M-08	08.85	11.85	23231	45259	571	500-592	599	822	Productive
M-010	01.86	06.86	22634	46446			1515	820	Non-productive
M-012	07.86	12.87	24084	45447			1970	814	Monitoring
M-013	06.85	11.85	23236	46095	1028	910-1951	2070	802	Productive
M-014	01.86	05.86	22881	45499	474	441-1004	1004	772	Productive
M-016	06.86	09.86	23181	45432	---	0-832	846	789	Productive
M-018	09.86	06.87	22936	44373			1857	894	Monitoring
M-019	07.87	01.88	21528	45003			1550	758	Monitoring
M-020	01.88	06.88	21525	45545			1530	768	Monitoring
M-021	06.88	11.88	21541	45994			1518	717	Non-productive
M-029	07.88	01.89	25428	45964			1514	771	Non-productive
M-037	08.87	01.88	23805	47073			1771	863	Monitoring
M-042	07.88	01.89	24087	46871			1800	844	Monitoring
M-044	01.90	06.90	25229	45912			2256	782	Monitoring
M-045	09.90	05.91	21522	45756			2150	710	Productive

3.2 Evaluation of formation temperatures and reservoir pressures

In order to estimate formation temperatures and pressures in Mutnovsky, the wells were divided into six groups (Figure 3). Each group contains three to six wells located close to each other and, therefore, assumed to have similar thermodynamic conditions. This grouping of wells was necessary since only limited temperature and pressure data were available for each well and, furthermore, as most of the temperature and pressure measurements were carried out during flow tests or immediately after them.

A similar procedure was used to estimate both formation temperatures and pressures for the individual well groups. First of all, the downhole measurements for all the wells in the group were drawn in the same scale. Secondly, pressure and temperature data were drawn together on the graphs. Thirdly, the boiling curve temperature and pressure with depth were drawn in the same scale on a separate sheet. When all these graphs were at hand for a selected group of wells, they were layed on top of each other on an illuminated surface and a single formation temperature profile defined for the wells in the group. The initial pressure estimate needed special treatment. In cases of wells where a boiling curve with depth conditions exist, the pressure is defined in the interval of this curve. Beneath it and down to the wellbottom, a pressure estimate was based on water density according to the predefined formation temperature profile. For wells of no boiling, the pressure was estimated from water level data and water density based on the formation temperature. It should be noted that the pressure estimate is of limited quality due to scarce downhole pressure data and low resolution in the depth scale. This may easily lead to inaccuracy on the order of $\pm 2-4$ bars.

In the following text a short description is given on the formation temperatures and pressures in each well group. Table 2 shows the numerical values of formation temperatures and pressures at selected depths.

Group 1: This group includes wells Mv-1, M-1, M-08, M-013, M-014 and M-016. All of them except well M-013 detected a steam zone in the upper part of the reservoir. Figures 4 and 5 show temperature profiles in wells M-1 and M-013 and the estimated formation temperature. Figure 4 shows that the steam zone ranges from 250 to 600 m depth. All the measurements in well M-1 were carried out during one year warm-up period after extensive flow tests. Above the steam zone the estimated formation temperature corresponds to the boiling curve with depth and also below 600 down to 950 m. At greater depths, the temperature profile indicates saturated single-phase liquid zone. The formation temperature in this zone is based on drilling data obtained before the flow test showing higher temperature values than after the flow test. The pressure below 950 m depth was calculated using the formation temperature profile and the PREDYP computer program (Arason and Bjornsson, 1993).

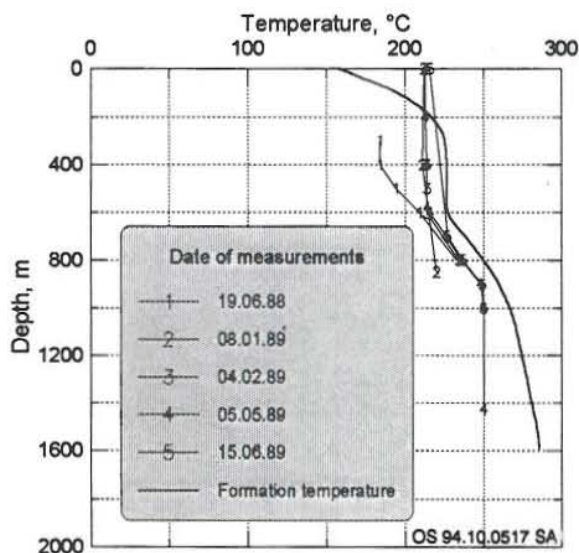


FIGURE 4: Formation temperature for well M-1

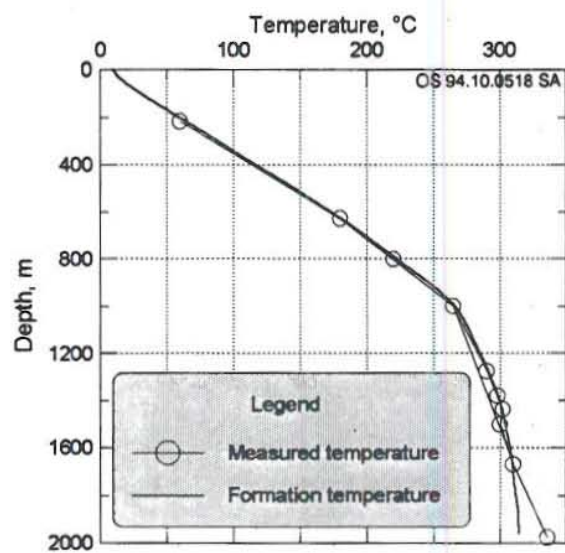


FIGURE 5: Formation temperature for well M-013

TABLE 2: Numerical values for estimated formation temperatures and reservoir pressures in Mutnovsky wells. The pressure is in bar-g

GROUP 1					GROUP 2				
Elevation (m a.s.l.)	M-1		M-013		Elevation (m a.s.l.)	M-24		M-012	
	T (°C)	P (bar)	T (°C)	P (bar)		T (°C)	P (bar)	T (°C)	P (bar)
600	214	21	57	---	600	210	18.1	87	---
400	227	26.4	114	3.1	400	234	29.1	135	---
200	228	26.5	171	21.2	200	235	29.7	181	12.5
0	247	36.9	220	38.5	0	248	37.5	220	29.5
-200	265	52.3	265	54.4	-200	265	52.3	236	45.9
-400	274	66.5	284	67.3	-400	270	67.5	242	61.9
-600	280	82.4	299	83.8	-600	280	82.5	245	77.9
-800	285	97.1	307	97.3	-800	---	---	247	96.6
-1000	---	---	312	111.1	-1000	---	---	250	112.5
GROUP 3					GROUP 4				
Elevation (m a.s.l.)	M-07		M-044		Elevation (m a.s.l.)	M-30		M-037	
	T (°C)	P (bar)	T (°C)	P (bar)		T (°C)	P (bar)	T (°C)	P (bar)
600	37	---	21	---	600	50	---	42	---
400	82	---	44	---	400	127	---	86	---
200	148	9.6	79	3.0	200	202	13.5	202	15.3
0	208	27	130	21.8	0	236	30.1	239	31.9
-200	237	43.4	176	39.8	-200	256	46.0	257	47.0
-400	242	59.4	202	57.0	-400	266	61.3	265	62.4
-600	242	75.4	218	73.8	-600	272	76.5	270	77.6
-800	---	---	222	90.4	-800	274	91.4	271	92.7
-1000	---	---	221	107	-1000	---	---	---	---
GROUP 5					GROUP 6				
Elevation (m a.s.l.)	M-01		M-018		Elevation (m a.s.l.)	M-010		M-020	
	T (°C)	P (bar)	T (°C)	P (bar)		T (°C)	P (bar)	T (°C)	P (bar)
600	31	---	51	---	600	39	---	48	---
400	124	1.4	105	---	400	103	---	102	4.5
200	209	17.8	195	13.0	200	164	15.4	156	22.8
0	242	33.8	236	30.3	0	218	32.5	208	40.2
-200	265	50.0	258	47.0	-200	249	48.6	250	56.4
-400	282	65.3	264	62.0	-400	257	64.2	275	71.7
-600	295	79.1	267	77.3	-600	262	79.62	293	86.3
-800	---	---	269	92.7	-800	---	---	306	100.2
-1000	---	---	272	107.9	-1000	---	---	321	113.7

The temperature profile of well M-013 is of a gradient type with signs of convective zone below 1000 m until the well's bottom (about 2000 m) where the temperature reaches 320°C (Figure 5). This well is located outside the steam zone area, about 500 m to the east of well M-1 and is characterized by single-phase liquid conditions. The estimated formation temperature and the reservoir pressure in this well corresponds to the measured values.

Group 2: This group includes wells Mv-2, M-13, M-24, M-26, M-03 and M-012. Figure 6 shows a single profile for each of the wells Mv-2, M-24 and M-26 all together and Figure 7 shows several temperature profiles for well M-012. Four wells of this group, (Mv-2, M-24, M-26 and M-03), have very similar conditions as the wells in the first group which detected steam zone in the reservoir. Therefore, the formation temperature curve has a similar shape, boiling curve with depth down to 250 m; steam zone in the 250-700 m interval; boiling curve with depth at 700-1000 m and below that a single-phase liquid zone. Two wells in this group are located farther to the north and do not detect the steam zone. These wells are M-13 and M-012. The formation temperature of well M-13 corresponds to boiling curve with depth from 500 m to the bottom of the well (800 m). The downhole temperature of well M-012 (Figure 7) is lower than in any other well in the group and indicates single-phase liquid conditions and convective heat transfer in the depth range from 800 m to the bottom of the well at 2000 m.

Group 3: This group includes wells M-07, M-029 and M-044. They are located in the northern part of the wellfield. Figures 8 and 9 show temperature profiles measured in wells M-07 and M-044 and estimated formation temperatures. This area is colder north of the Shirotny fracture (Figure 3) and also colder than in the area of group 2, suggesting limited flow across the fault to the north. Estimated formation temperatures and pressure in these wells correspond to the logging data.

Group 4: This group is represented by wells M-30, M-037 and M-042 which are located along the northeastern striking low-resistivity branch. Figures 10 and 11 show temperature profiles in wells M-037 and M-042. The formation temperature is characterized by boiling from 450 to 900 m for wells M-037, M-042 and at 400-500 m for well M-30. The formation temperature for well M-037 below 900 m was estimated by using the program BERGHITI where the thermal recovery data were available (Helgason, 1993). The pressure below 900 m was calculated by using the PREDYP program.

Group 5: This group of wells (M-01, M-04, M-018, M-17 and M-42) is located 500 m southwest of group 1. Figures 12 and 13 show temperature data in wells M-04 and M-17. The temperature profiles from all the

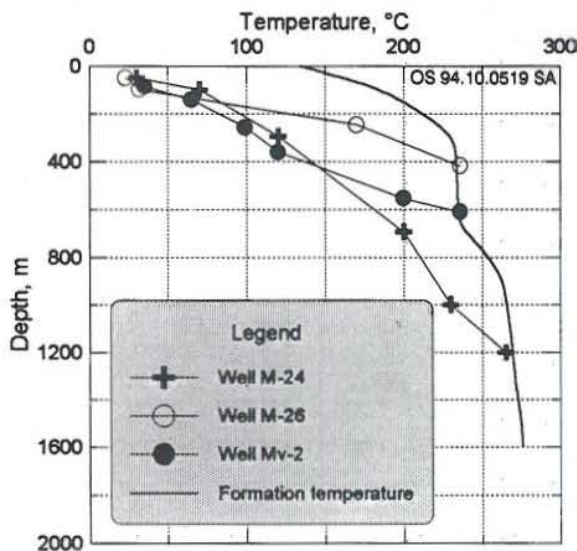


FIGURE 6: Formation temperature for wells M-24, M-26 and Mv-2

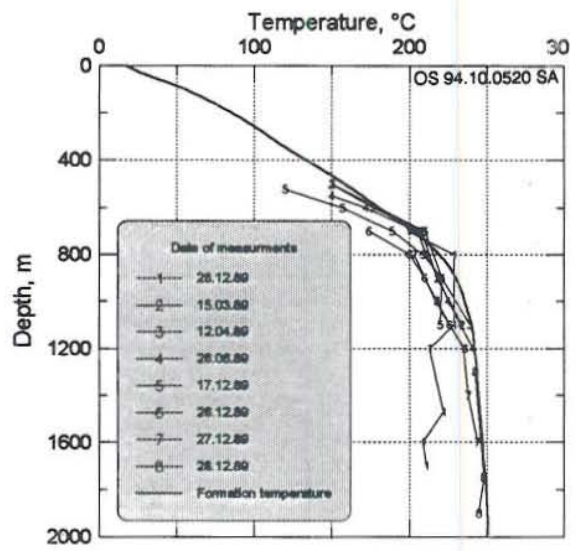


FIGURE 7: Formation temperature for well M-012

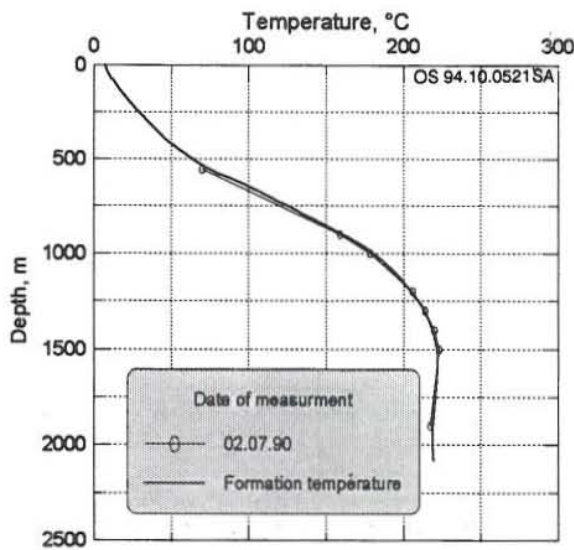


FIGURE 8: Formation temperature for well M-044

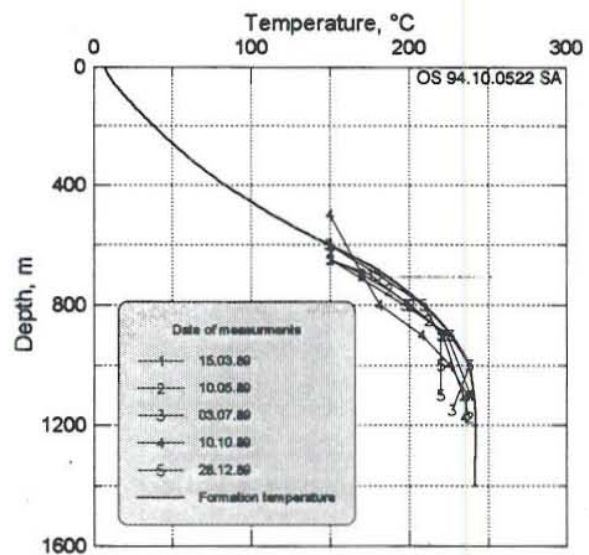


FIGURE 9: Formation temperature for well M-07

wells in this group are characterized by a boiling curve with depth conditions in the depth range 400-1000 m and for well M-01 at 400-1100 m. The estimated formation temperatures and reservoir pressures for wells M-17, M-42 and M-018 correspond to the logging data, but estimated values for wells M-01 and M-04 correspond to the logging data only down to sea level. At greater depths the measured well temperatures are disturbed by flow testing, therefore, the temperatures at 800-2000 m were estimated using temperature values obtained right after drilling.

Group 6: This group includes wells M-010, M-019, M-020, M-021 and M-045. Figures 14 and 15 show downhole data from well M-010 and in wells M-019, M-021 and M-045 all together. The wells are located near the southern boundary of the wellfield except well M-010 that is at the eastern wellfield boundary. The estimated formation temperatures and pressures of these wells correspond to logging data. The downhole temperatures and pressures of wells M-019, M-020, M-021 and M-045 show, however, boiling conditions in the deeper part of the reservoir, in the depth range 1700-2000 m.

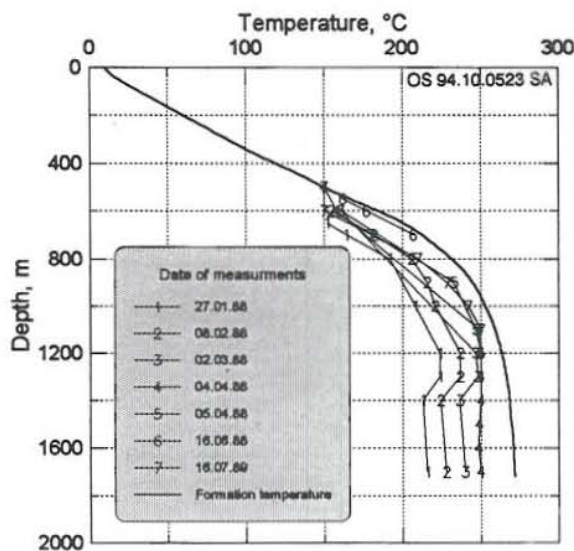


FIGURE 10: Formation temperature for well M-037

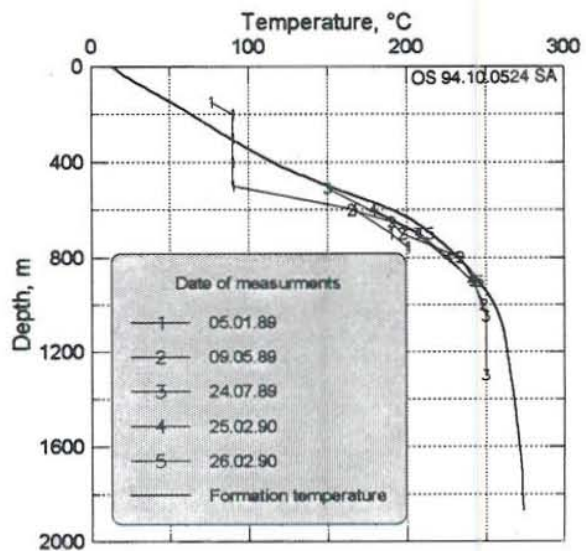


FIGURE 11: Formation temperature for well M-042

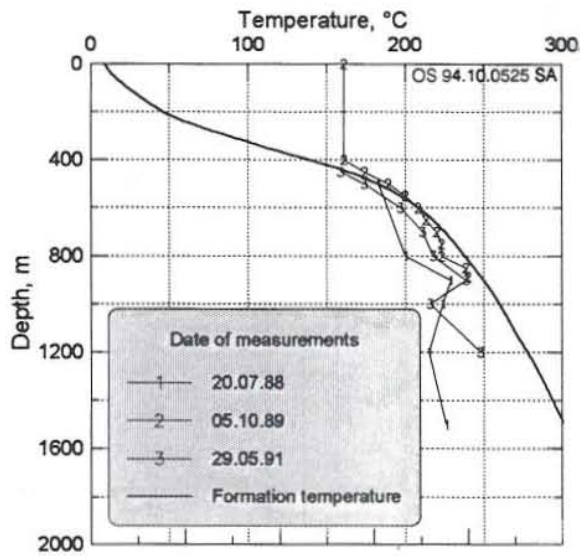


FIGURE 12: Formation temperature for well M-04

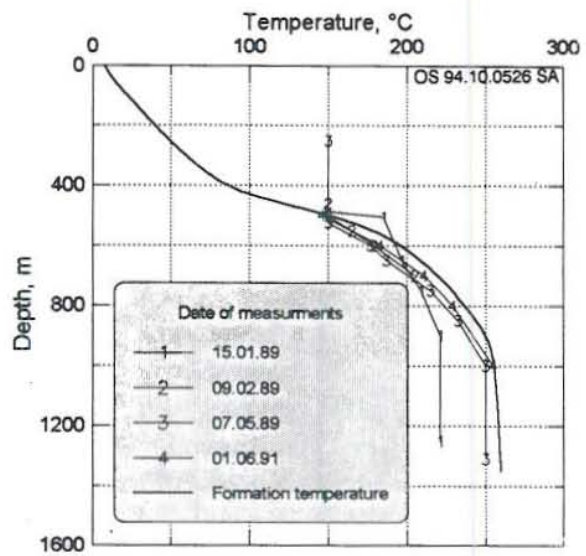


FIGURE 13: Formation temperature for well M-17

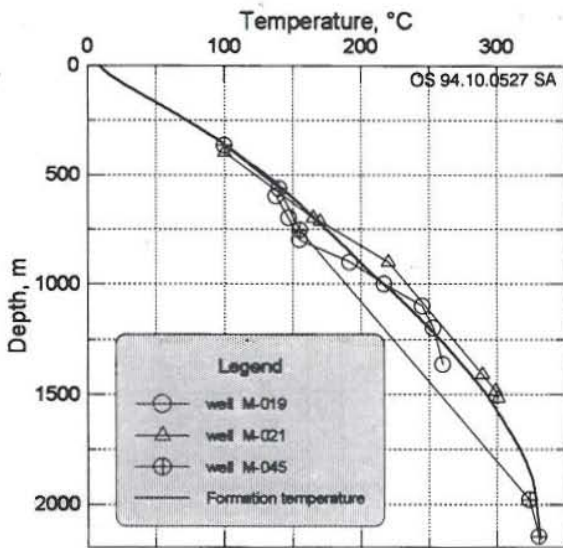


FIGURE 14: Formation temperature for wells M-019, M-021 and M-045

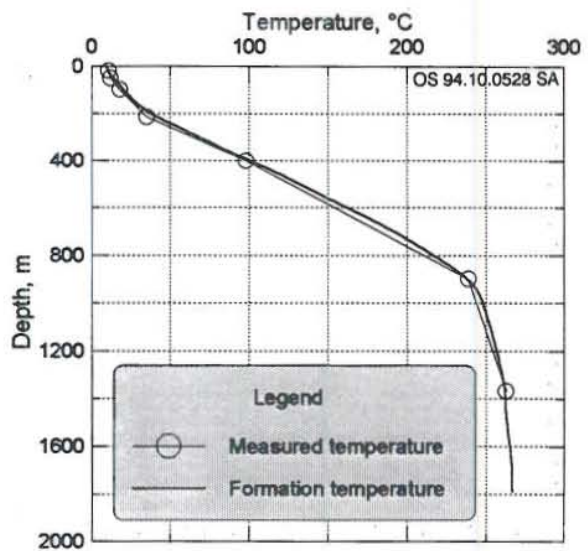


FIGURE 15: Formation temperature for well M-010

3.3 Temperature and pressure distribution in the Mutnovsky reservoir

Figures 16 and 17 show the estimated formation temperature and reservoir pressure distribution at -600 m a.s.l. and Figure 18 shows a temperature cross-section through the wellfield from south to north. Several additional temperature maps and cross-sections are presented in Appendix I.

Both the temperature and the pressure contours, in Figures 16 and 17, indicate a flow of geothermal fluid from south to north. The contours are open in the south where the maximum temperature and pressure values

are observed. This anomaly of high temperature and pressure extends towards north, up to the first well group where the contours change direction to northeast and have an open boundary in the northeastern part of the wellfield. The temperature cross section of Figure 18 shows a similar trend. The highest temperature at depth is found to the south. However, at shallow depth a temperature maximum coincides with the steam zone at the centre of the wellfield, indicating good vertical permeability close to the surface.

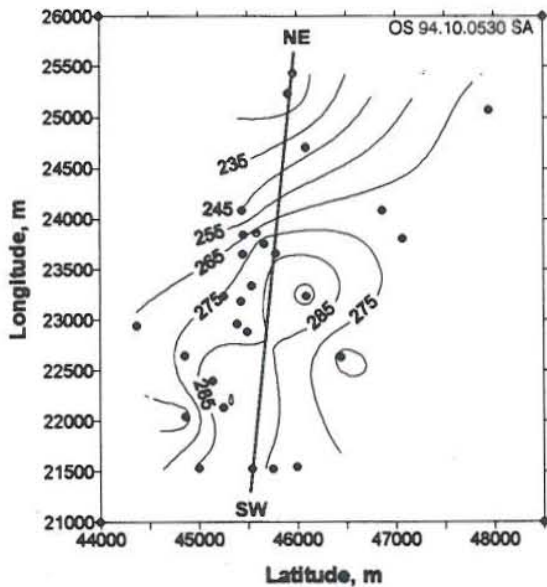


FIGURE 16: Temperature contours (°C) at -600 m a.s.l.

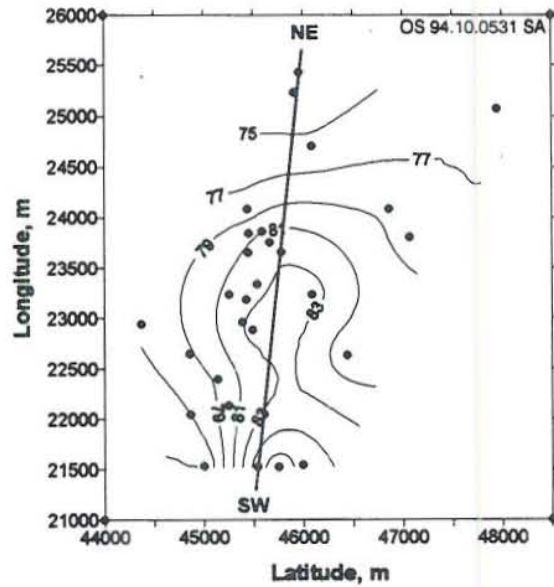


FIGURE 17: Pressure contours (bar-g) at -600 m a.s.l.

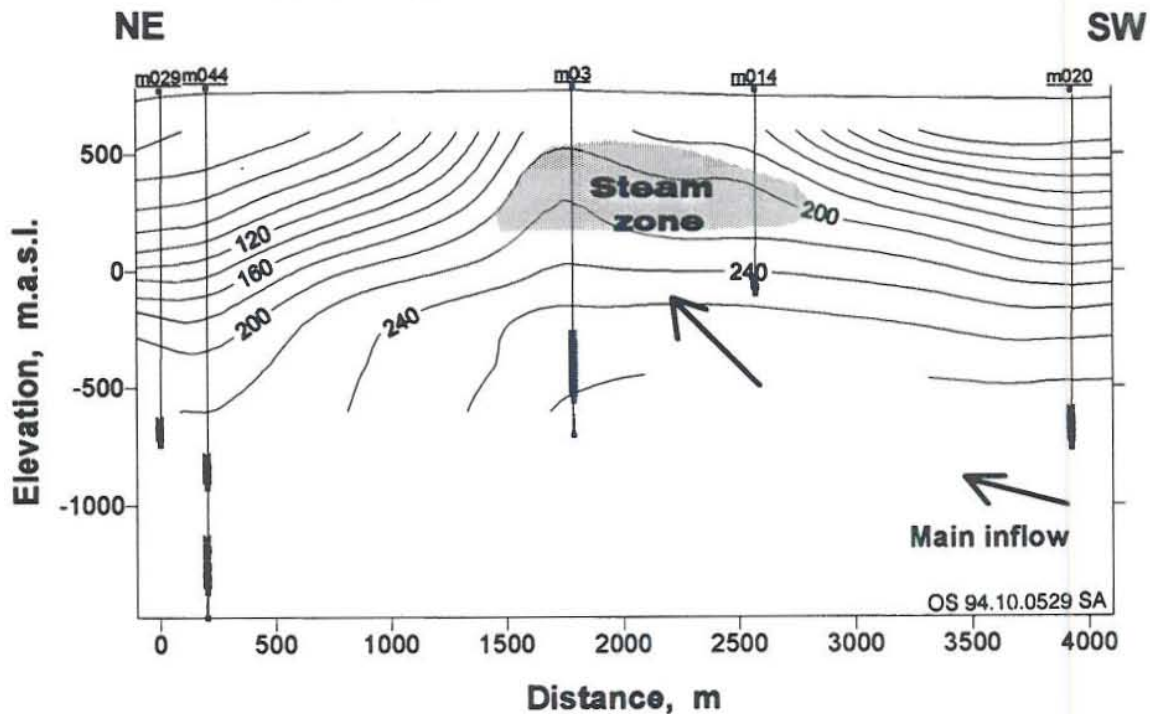


FIGURE 18: A N-S temperature cross-section through wells M-029, M-044, M-03, M-014 and M-020; permeable intervals in the wells are shown with bold lines

It should be noted that no reversed temperature profiles have been identified in the field except possibly for well M-044. Therefore, the main flow seems to be controlled both by vertical and horizontal flow paths. In the south, at depth greater than -800 m a.s.l, the pressure and the temperature follow the boiling curve with depth; but in the central part of the wellfield, the boiling curve with depth conditions reside between the water level (~ 400 m a.s.l.) approximately down to the sea level.

4. EVALUATION OF PRODUCTION DATA

4.1 Data from a two year long extensive flow testing

The productive Mutnovsky wells have all undergone flow tests lasting from several days to years. The short flow tests have been carried out in order to estimate fluid properties and to calculate permeability by using pressure build-up data and the Horner plot method. A long term flow test was carried out during 1987-1988, using nine wells as producers (Kiryukhin, 1992; 1993). The purpose of the test was to assess the geothermal reserves of the Mutnovsky field. The productive wells can be divided into two groups according to their flow characteristics:

- The steam zone wells that intersected a steam cap over liquid-dominated the reservoir. They are mostly shallow (less than 800 m) and are characterized by high discharge enthalpy;
- The single-phase liquid zone wells are deep (1500-2500 m) and produce fluid of lower enthalpy than in the steam zone wells. These wells need to be compressed by air in order to discharge.

The production data from the two-year long extensive flow tests is summarized in Table 3. The total flow rate of the fluid decreased as well as the wellhead pressure in all of the wells except well M-014 where the total flow rate increased, while the fluid enthalpy decreased. This well is located at the southern edge of the steam zone and these changes can be explained as a recharge of lower enthalpy fluid into the steam zone. Well M-1 also increases apparently in flow rate, but this is due to reduced wellhead pressure.

TABLE 3: Production data collected in flowing wells during an extensive flow test from January 1987 (initial) to September 1988 (final)

Well	Wellhead pressure (bar-g)		Total flow (kg/s)		Steam flow (kg/s)		Dryness (%)		Enthalpy (kJ/kg)	
	Initial	Final	Initial	Final	Initial	Final	Initial	Final	Initial	Final
Mv-2*	5.7	5.1	4.4	3.2	2.8	2.2	63	69	1979	2095
M-1	10.3	6.8	8.6	20.6	2.1	6.9	24	33	1250	1375
M-24	5.6	6.1	36.5	33.2	9.5	10.2	26	30	1203	1298
M-26*	6.1	6.1	24.4	19.3	21.7	17.2	88	89	2500	2527
M-01	6.3	6.2	56.8	50.8	17.5	18.2	31	36	1323	1425
M-08*	5.9	6.1	5.7	3.6	5.1	3.3	89	92	2525	2568
M-013	6.3	7.9	33.6	31.3	11.1	11.3	33	36	1365	1456
M-014*	6.7	6.1	7.2	9.3	5.0	5.3	69	57	2118	1860
M-016*	6.1	5.8	25.6	21.2	22.8	19.6	89	92	2527	2589

* - Steam zone wells

The changes in the fluid enthalpy were different for wells in the steam zone compared to wells fed by the single-phase liquid zone. The enthalpy of the fluid increased only slightly for the steam zone wells except for well M-014 where the enthalpy decreased from 2118 to 1860 kJ/kg. The changes of fluid enthalpy were more significant for wells producing from the single-phase liquid zone, where it increased with time in all cases. This enthalpy increase is easily explained by induced boiling in the reservoir during production.

4.2 Computed downhole conditions during flow

In order to analyse the enthalpy change in wells producing from the single-phase liquid zone the wellbore simulator HOLA was applied to predict downhole conditions in some of the wells (Bjornsson and Bodvarsson, 1987). Four wells were studied, wells M-1, M-01, M-013 and M-24. These wells produced fluid with enthalpy higher than the estimated liquid water enthalpy at the individual feedzones. Table 4 compares the initial reservoir enthalpy with the flow test data.

TABLE 4: Enthalpy of wells before and during flow testing

Well	Formation temperature at a major feed zone (°C)	Corresponding liquid enthalpy (kJ/kg)	Measured wellhead enthalpy (kJ/kg)	
			Initial	Final
M-1	280	1236	1250	1375
M-01	285	1263	1323	1425
M-013	300	1345	1365	1456
M-24	280	1236	1203	1298

Figure 19 shows as an example the calculated downhole conditions of well M-24. As input data, the wellbore simulator requires only the wellhead parameters (total flow, enthalpy and pressure) and the wellbore geometry for predicting the downhole conditions. The upper part of Figure 19 shows the calculated temperature and pressure early in the flow test. At this time the wellhead enthalpy was similar to the reservoir enthalpy estimated from the formation temperature analysis. The simulations predict flashing in the wellbore, 100 m above the bottom of the well. The lower part of Figure 19 shows calculated downhole conditions based on the wellhead enthalpy measured late in the flow test. The figure shows that the well now flashes all the way down to the bottom, indicating that boiling starts within the formation before the fluid enters the well.

The main conclusion of this study is that flashing all the way into the formation during discharge is quite possible for the Mutnovsky wells. This also leads to the important conclusion that increased enthalpy of production wells is to be expected in the future as the reservoir pressure draw-down increases and the steam zone as well as the two-phase reservoir zone will expand accordingly.

4.3 Reservoir permeability

The permeability thickness (kh) has been estimated for most of the Mutnovsky wells. The analysis is based on either pressure build-up data collected after flow or on injection tests carried out during well completion. Table 5 shows the estimated values of the permeability-thickness. Fractures are assumed to play a major role in the permeability distribution within the Mutnovsky reservoir. This is reflected on values of the permeability-thickness. They are substantially higher for wells intersecting the north and northeast trending fault zones and lower for wells located outside or at the boundaries of the fault zones. This reflects the importance of vertical fractures for the fluid flow pattern within the reservoir.

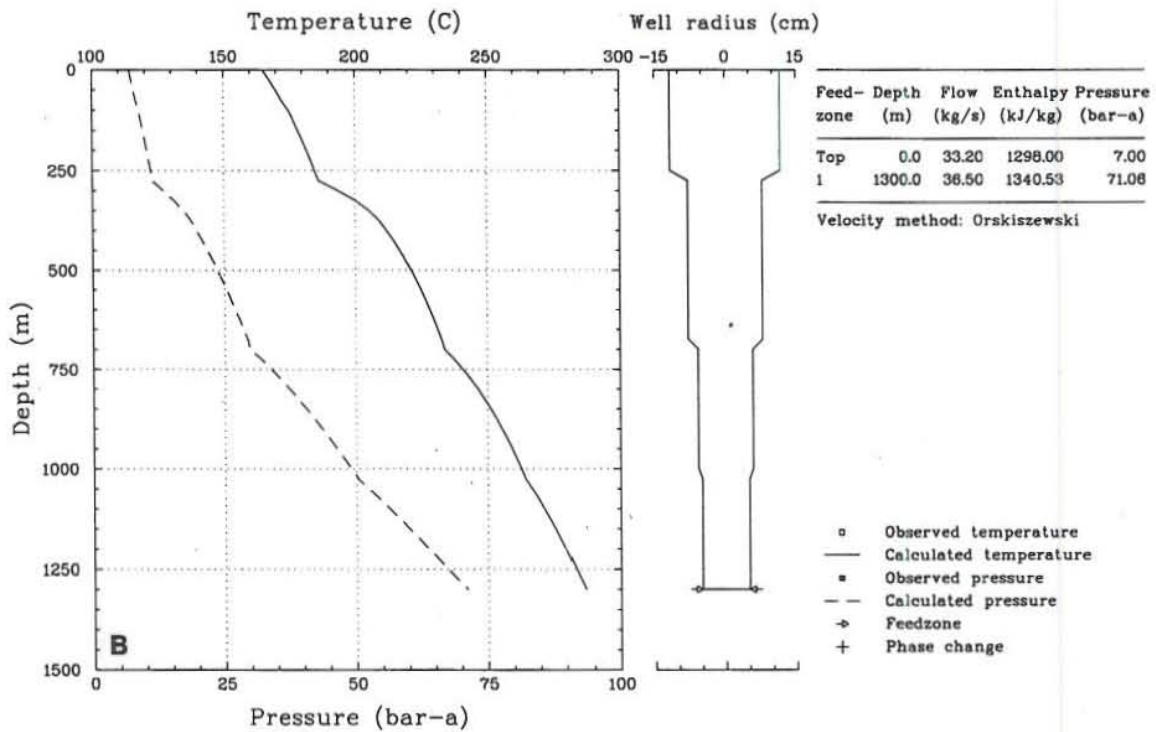
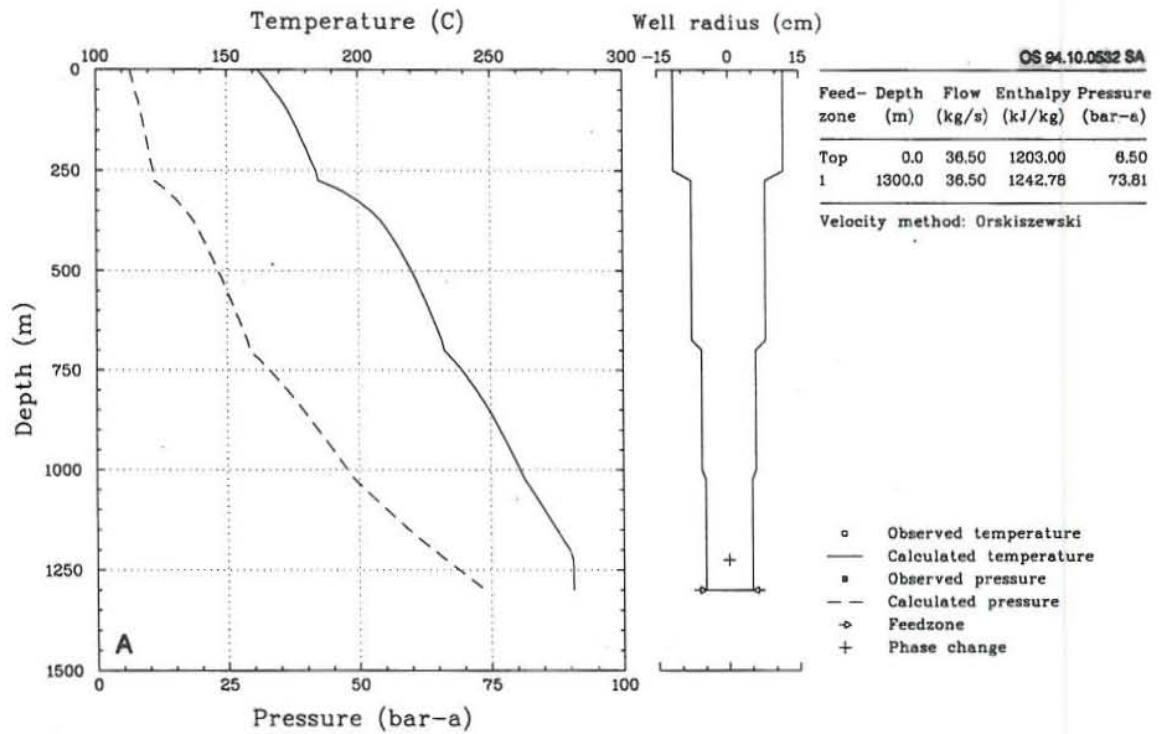


FIGURE 19: Simulation of the downhole conditions during flow test for well M-24, a) in the beginning of the flow test; b) at the end of the flow test

TABLE 5: Calculated permeability thickness (kh) of Mutnovsky wells

Well	Group 1		Group 3			Group 4		
	M-1	M-013	M-07	M-044	M-029	M-30	M-042	M-037
Permeability-thickness (Dm)	1.61	3.2	0.28	0.13	0.11	0.61	1.64	0.54
Well	Gr.2	Group 5			Group 6			
	Mv-2	M-01	M-04	M-018	M-019	M-020	M-021	M-045
Permeability-thickness (Dm)	4.46	1.51	0.17	0.42	0.04	0.78	1.27	1.65

5. A CONCEPTUAL RESERVOIR MODEL FOR THE MUTNOVSKY FIELD

In the previous chapters, a summary is given on the geological and geophysical studies conducted in the Mutnovsky field. The reservoir pressures and formation temperatures were evaluated and production characteristics of the wells were discussed. In Figure 20, an attempt is made to incorporate the results of these studies into a single conceptual model for the Mutnovsky geothermal system. The main parts of the model are as follows:

1. The Mutnovsky reservoir is an open geothermal system with main inflow from the south and main outflow towards northeast. The reservoir is of an elongated shape corresponding to the major fault zone in the area. These conclusions are based on the temperature and pressure distribution within the reservoir.
2. The southern boundary of the reservoir is an open boundary and it is assumed to be south of wells M-045, M-019, M-020 and M-021. Another open boundary is located towards the northeast, close to well M-30. The Shirotny fracture is assumed to form the northern boundary of the reservoir. This is based on the fact, that permeability-thickness and temperature decrease rapidly north of the Shirotny fracture. The eastern and western boundaries of the reservoir are also assumed to be closed and located on both sides of the faults trending north and northeast.
3. The main upflow zone is located in the south of the reservoir and is believed to be underneath the Mutnovsky volcano. The upflow temperature is higher than 300°C.
4. The formation temperature and pressure of wells indicate a flow along the fractures from south to north. The flow changes direction towards northeast in the central part of the wellfield. This is due to young and active faults of that direction in this area.
5. A comparison of the pressure and temperature data indicates that the reservoir is in liquid state except for the upper part. There, the reservoir conditions are characterized by free surface and boiling curve with depth exists several hundred meters down. A steam zone exists in a limited volume of the reservoir where two of the major fault zones of north and northeast orientation intersect each other.
6. The static water level in the reservoir is relatively low. Therefore, the recharge into the reservoir is lower than the outflow and discharge to the surface.
7. The reservoir is of a low permeability, between 10-30 mD. The permeability is mostly secondary due to tectonic faulting and fracturing.

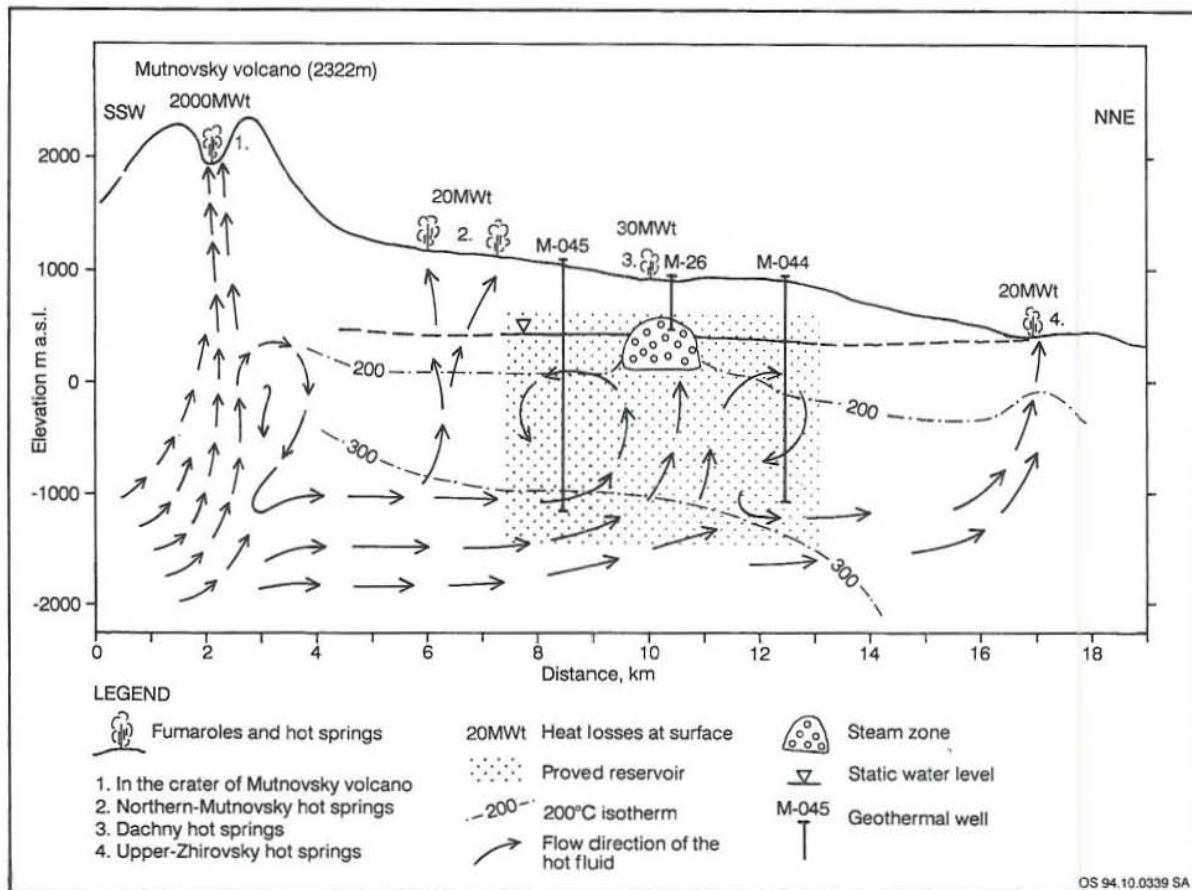


FIGURE 20: A conceptual model of the Mutnovsky geothermal field

6. GENERAL RESERVOIR ASSESSMENT FOR THE MUTNOVSKY FIELD

The general reservoir assessment is mainly based on a rough calculation on the available heat which is contained initially in the fluid and rocks of the reservoir. In this chapter, two alternatives are used to estimate the production capacity of the Mutnovsky reservoir. The first one is to estimate the reserves of available energy in a general volumetric assessment. As several of the factors used for the estimate are only known approximately the second estimate is based on an attempt to define the accuracy of the calculations by applying random distribution in some of the reservoir properties. This is the so-called Monte Carlo probability method.

6.1 Volumetric analysis

The volumetric method estimates the "stored heat" contained in the subsurface fluids and rocks, assuming a homogenous and closed reservoir (no recharge). It is considered to be a rather limited but inexpensive method for roughly estimating the power potential of a geothermal reservoir. The governing equation for estimating the total heat available from a reservoir volume is (Bjornsson, 1994)

$$E_s = E_r + E_f = V\rho_r C_r (1-\phi)(T-T_r) + V\rho_f \phi (h-h_r) \tag{1}$$

where

- $E_{s,r,f}$ = stored heat in the system, rock and fluid, respectively;
- V = reservoir volume;
- ϕ = rock porosity;
- T, T_r = temperature, reference temperature;
- C_r = rock heat capacity;
- $\rho_{r,f}$ = density of rock and fluid, respectively;
- h, h_r = enthalpy of fluid at initial and reference reservoir temperature.

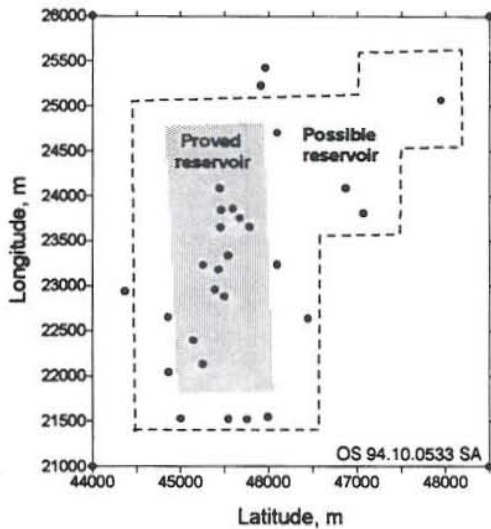


FIGURE 21: The contours of the proven and the possible reservoir area in the Mutnovsky geothermal field

The governing parameter in the above equation is the reservoir volume. In many cases, only the subsurface conditions in a small wellfield are known, although the reservoir may be much larger. This uncertainty has led to the definition of proven and possible reservoirs (Sarmiento, 1993). In this work, the central part of the wellfield in Figure 21 is considered as the proven reservoir, whereas the possible reservoir area is the central and northeastern sites of the wellfield.

Table 6 presents values of the proven and possible reservoir volumes for the Mutnovsky geothermal area and the mean initial temperature.

to 25% of the stored heat under general conditions of porosity and permeability. However, in some natural systems it is substantially lower, approaching zero for impermeable rocks. It should be emphasized that this recovery amounts only to the heat stored above the reference temperature, T_r in Equation 1, which is assumed to be 200°C in the following calculations.

The stored heat calculated by the above equation must be converted into useful thermal energy by applying an empirical factor, the so-called Recovery Factor. This factor generally ranges up

TABLE 6: Numerical values used to calculate the stored heat in the Mutnovsky reservoir

Parameter	Proven	Possible
Area (km ²)	3	9
Thickness (m)	1500	1500
Porosity (%)	10	10
Temperature (°C)	280	270
Rock density (kg/m ³)	2850	2850
Specific heat (kJ/[kg °C])	0.9	0.9

In order to obtain a rough estimate for the recovery factor for the Mutnovsky field, the system was considered closed and the total mass and the possible heat yield estimated for a chain of conditions. Initially, before production starts, the reservoir is considered liquid saturated with 100 bar-a pressure (P_1). The liquid state remains until the reservoir reaches 64 bar-a pressure (P_2) which is the saturation pressure of water at 280°C in the case of the proven area or until the 55 bar-a (saturation pressure of water at 270°C) in the case of the possible area. The mass withdrawn through this state by expansion of the fluid is estimated as

$$M = V\rho_w [\phi c_w + c_r (1-\phi)](P_1 - P_2) \quad (2)$$

Substituting values for both areas, and considering compressibilities of water, c_w and rock, c_r , as 3.0×10^{-9} and $0.7 \times 10^{-9} \text{ Pa}^{-1}$, respectively, the mass withdrawn, M , and heat yielded, Q_e , will be for the proven area:

$$M^{Proven} = 4.5 \times 10^9 \times 750.5 [(0.3 + 0.63) \times 10^{-9}] (100 - 64) \times 10^5 = 1.13 \times 10^{10} \text{ kg} \quad (3)$$

$$Q_e^{Proven} = 1.13 \times 10^{10} \times 1236.8 = 14.0 \times 10^{12} \text{ kJ} \quad (4)$$

and for the possible area, respectively:

$$M^{Possible} = 13.5 \times 10^9 \times 767.8 [(0.3 + 0.63) \times 10^{-9}] (100 - 55) \times 10^5 = 4.34 \times 10^{10} \text{ kg} \quad (5)$$

$$Q_e^{Possible} = 4.34 \times 10^{10} \times 1185.2 = 51.4 \times 10^{12} \text{ kJ} \quad (6)$$

During the next production stage the reservoir is believed to produce only steam. These conditions are maintained down to 15.5 bar-a pressure (200°C temperature) which is the estimated minimum reservoir pressure that allows discharge from the wells. This value was estimated by the following equation:

$$P_{\min} = (\text{Depth to major feed zone}) \times (\text{Pressure losses in the hole}) + (\text{Wellhead pressure}) \quad (7)$$

$$P_{\min} = 2500 \times 0.34 \text{ bar}/100 \text{ m} + 7 = 15.5 \text{ bar-a} \quad (8)$$

At this time the volume saturation of steam in the reservoir S , is given by (Bjornsson, 1993):

$$S = 1 - \frac{\phi \rho_{w1} (h_{s1} - h_{w2}) - \alpha_r C_r \rho_r (1-\phi)(T_1 - T_2)}{\phi \rho_{w2} (h_{s2} - h_{w2})} \quad (9)$$

where the subscripts 1 and 2 refer to saturation values at the initial pressure and at the minimum pressure (15.5 bars), respectively and α_r means the part of the reservoir that takes place in the heat exchange with fluid. The last parameter can be estimated as

$$\alpha_r = m_f / m_r \quad (10)$$

where m_f is the depth interval of permeable feedzones in wells and m_r is the total reservoir thickness. This factor is assumed 0.05 for the proven reservoir and 0.03 for the possible reservoir.

Substituting values into the above equation gives the following saturation for the proven and possible areas:

$$S^{Proven} = 1 - \frac{0.1 \times 750.5 \times (2790 - 1237) - 0.05 \times 0.9 \times 2850 \times 0.9 \times 80}{0.1 \times 864.7 \times (2790 - 852)} = 0.36 \quad (11)$$

$$S^{Possible} = 1 - \frac{0.1 \times 767.8 \times (2790 - 1185.2) - 0.03 \times 0.9 \times 2850 \times 0.9 \times 80}{0.1 \times 864.7 \times (2790 - 852)} = 0.29 \quad (12)$$

These values give the withdrawal of steam during the boiling phase and for heat yielded through this process (Bjornsson, 1994):

$$M_S^{Proven} = V \times \phi \times (\rho_{w1} - (S \times \rho_{s2} + (1 - S) \times \rho_{w2})) = 8.7 \times 10^{10} \text{ kg} \quad (13)$$

$$Q_S^{Proven} = 8.7 \times 10^{10} \text{ kg} \times 2790 \text{ kJ/kg} = 242.7 \times 10^{12} \text{ kJ} \quad (14)$$

$$M_S^{Possible} = V \times \phi \times (\rho_{w1} - (S \times \rho_{s2} + (1 - S) \times \rho_{w2})) = 20.5 \times 10^{10} \text{ kg} \quad (15)$$

$$Q_S^{Possible} = 20.5 \times 10^{10} \text{ kg} \times 2790 \text{ kJ/kg} = 572 \times 10^{12} \text{ kJ} \quad (16)$$

Equations 4, 6, 14 and 16 provide an estimate for the total amount of heat produced from the reservoir volumes. The value of the heat recovery factor follows as:

$$R_f = \frac{\text{Total heat yield}}{\text{Heat available}} = \frac{Q_e + Q_s}{V \rho_r C_r (1 - \phi)(T - T_r) + V \rho_f \phi (h - h_r)} \quad (17)$$

Substituting values into Equation 17 gives a recovery factor for the proven and for the possible reservoir as:

$$R_f^{Proven} = \frac{242.7 \times 10^{12} + 14.0 \times 10^{12}}{4.5 \times 10^9 \times 2850 \times 0.9 \times 0.9 \times (280 - 200) + 4.5 \times 10^9 \times 756.4 \times 0.1 \times (1236.8 - 852)} = 0.27 \quad (18)$$

$$R_f^{Possible} = \frac{572 \times 10^{12} + 51.4 \times 10^{12}}{13.5 \times 10^9 \times 2850 \times 0.81 \times (270 - 200) + 13.5 \times 10^9 \times 774.2 \times 0.1 \times (1185.2 - 852)} = 0.25 \quad (19)$$

The following equation applies for converting the heat reserve estimate into electrical energy (Sarmiento, 1993):

$$MW_e = \frac{\text{Heat available} \times \text{Recovery factor} \times \text{Thermal efficiency}}{\text{Load factor} \times \text{Life time}} \quad (20)$$

where the heat available is given by Equation 1, and the recovery factor by Equation 17. The value of the thermal efficiency for a condensing electrical turbine is assumed as 0.09. Additional load factor of 0.8 is also assumed and a 30 year life period for the power plant. The value of the life time in this equation is in seconds.

By inserting the numerical values, the following production capacities are assumed for the proven and for possible reservoir:

$$MW_e^{Proven} = \frac{962 \times 10^{12} \times 0.267 \times 0.09}{0.8 \times 30 \times 3.15 \times 10^{10}} = 30 \text{ MW} \quad (21)$$

$$MW_e^{Possible} = \frac{2529.5 \times 10^{12} \times 0.246 \times 0.09}{0.8 \times 30 \times 3.15 \times 10^{10}} = 74 \text{ MW} \quad (22)$$

The proven reservoir estimate is rather low due to the small area considered for the calculations. This is a pessimistic assessment and can be taken as the lower limit of the Mutnovsky production capacity.

6.2 Volumetric assessment by the Monte Carlo probability method

The previous study of the power potential of the Mutnovsky reservoir shows high uncertainty in several of the factors that serve as a base for the computations. In order to include this uncertainty in the computations, a method called Monte Carlo volumetric assessment has been proposed (Sarmiento, 1993). The basic equation of power output is the same as in the previous chapter, but this time a random probability is assigned to some of the reservoir properties.

The randomness of the uncertain values was defined either by square or triangular probability functions. Square probability distribution was assigned to the reservoir area and thickness, meaning that the minimum possible reservoir area is as likely as the mean and the maximum ones. The rock density, porosity, initial reservoir temperature and the plant life time were assumed to follow triangular distribution. This means that the likelihood of using either the minimum or the maximum value is negligible, whereas the mean value has the highest probability.

The procedure of calculating the production capacity of the Mutnovsky reservoir is as follows:

- 1) By using an Excel spread sheet, a 8 x 1000 matrix was created. Each column in this matrix contains random values of some reservoir property;
- 2) The power output was calculated according to Equation 1 by inserting the numerical values from the first line of the matrix. This was repeated 999 times for all the lines in the matrix;
- 3) The estimated production capacity was finally plotted as a histogram.

Tables 7 and 8 show the numerical values of the properties that are used for calculating the production capacity of the Mutnovsky reservoir and their probability distribution. Figures 22 and 23 show the results in histograms. According to this study, a 40-60 MW_e power plant seems reasonable for the proven reservoir and 70-100 MW_e for the possible reservoir.

TABLE 7: Best guess values and probability distribution for the proved reservoir calculations

Proved reservoir					
Property	Unit	Best guess (model)	Probability distribution		
			Type	From	To
Area	km ²	4.5	Square	3	5
Reservoir thickness	m	1850	Square	1000	2000
Rock density	kg/m ³	2730	Triangular	2700	3000
Rock specific heat	J/kg°C	900	Constant	---	---
Porosity	%	11	Triangular	2	18
Reservoir temperature	°C	280	Triangular	260	300
Reference temperature	°C	200	Constant	---	---
Water density at reservoir temp.	kg/m ³	756	Table, F(t)	791	715
Water enthalpy at reservoir temp.	kJ/kg	1234	Table, F(t)	1134	1343
Water density at reference temp.	kg/m ³	864.7	Constant	---	---
Water enthalpy at reference temp.	kJ/kg	852	Constant	---	---
Steam density at reference temp.	kg/m ³	7.9	Constant	---	---
Steam enthalpy at reference temp.	kJ/kg	2790	Constant	---	---
Recovery factor for reservoir	---	0.27	Constant	---	---
Thermal efficiency in turbine	---	0.09	Constant	---	---
Load plant factor	---	0.8	Constant	---	---
Plant life period	years	30	Triangular	25	30

TABLE 8: Best guess values and probability distribution for the possible reservoir calculations

Possible reservoir					
Property	Unit	Best guess (model)	Probability distribution		
			Type	From	To
Area	km ²	9	Square	6	10
Reservoir thickness	m	1310	Square	1000	2000
Rock density	kg/m ³	2771	Triangular	2700	3000
Rock specific heat	J/kg°C	900	Constant	---	---
Porosity	%	10	Triangular	2	18
Reservoir temperature	°C	272	Triangular	250	300
Reference temperature	°C	200	Constant	---	---
Water density at reservoir temp.	kg/m ³	770	Table, F(t)	791	715
Water enthalpy at reservoir temp.	kJ/kg	1194	Table, F(t)	1134	1343
Water density at reference temp.	kg/m ³	864.7	Constant	---	---
Water enthalpy at reference temp.	kJ/kg	852	Constant	---	---
Steam density at reference temp.	kg/m ³	7.9	Constant	---	---
Steam enthalpy at reference temp.	kJ/kg	2790	Constant	---	---
Recovery factor for reservoir	---	0.25	Constant	---	---
Thermal efficiency in turbine	---	0.09	Constant	---	---
Load plant factor	---	0.8	Constant	---	---
Plant life period	years	28	Triangular	25	30

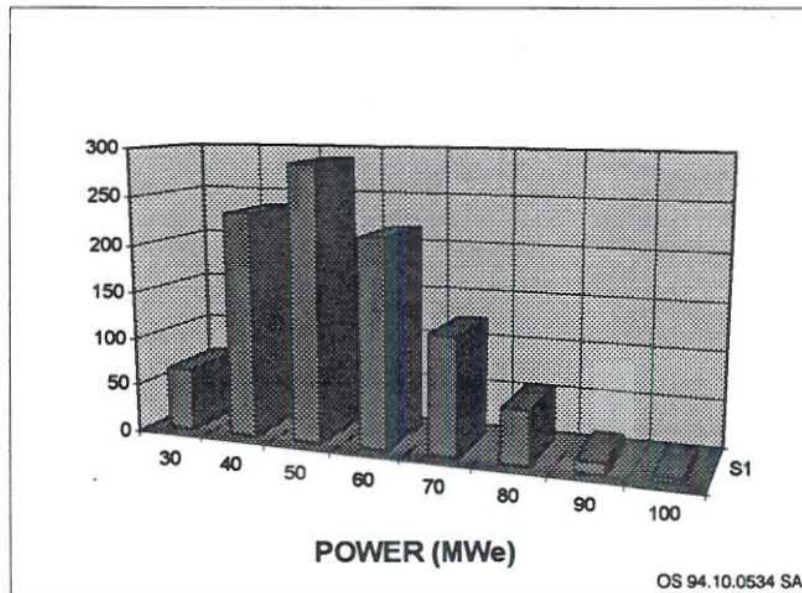


FIGURE 22: A frequency distribution for the available electrical power from the proven reservoir

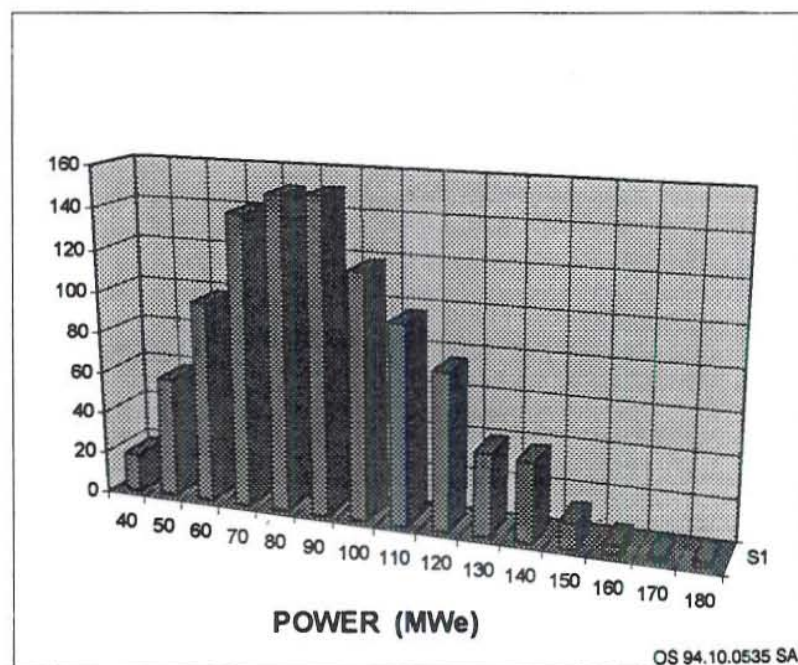


FIGURE 23: A frequency distribution for the available electrical power from the possible reservoir

7. CONCLUSIONS AND RECOMMENDATIONS

The main conclusions of this report are:

- a) The geoscientific information indicates that the subsurface flow paths in the Mutnovsky area are controlled by two main fault systems oriented from south to north and from southwest to northeast.

A recharge of $\geq 300^{\circ}\text{C}$ liquid fluid is at the south part of the reservoir and the main upflow zone is assumed to be underneath the Mutnovsky volcano, 8 km south of the present wellfield. The flow from south follows the meridional fault zone towards the wellfield, where it changes direction to northeast due to the SW-NE directing faults in this region.

- b) The Mutnovsky reservoir is a liquid-dominated system with a steam zone in the upper part of the central area of the wellfield. The liquid part of the reservoir is close to boiling conditions and during discharge boiling occurs in the feed zones of the wells as indicated by wellbore simulations and well test analysis. This will eventually lead to the expansion of the steam zone and the two-phase zone in the reservoir during production.
- c) Only limited production data were available for this study. That is why, only a general reservoir assessment by using volumetric calculations and Monte Carlo probability method are presented in this report. These calculations suggest, that the possible power potential of the Mutnovsky geothermal field is between 70-100 MW_e. These values for the generating capacity are similar to results previously obtained by Russian engineers (Perveev et al., 1992).

The layout of the production wells for a future electrical power plant is a very important part of the reservoir exploitation. The best locations for production wells are within the area that is overlying the steam zone of the reservoir. Although, the production data of some wells discharging dry steam show decreasing fluid enthalpy during two years of flow testing, the steam zone will provide dry steam for electrical power generation for several years of operation. At this moment, a lot of questions are unanswered about how much and for how long a time, the steam zone can provide dry steam before the reservoir rocks are cooled down due to flashing of reservoir fluids and due to liquid recharge from the surrounding parts of the reservoir. Numerical modelling of the Mutnovsky geothermal field will address such questions and should become an essential part of the development of the field.

The following list suggests some items that may lead to more accurate results from numerical simulation studies. They are:

1. More temperature and pressure logs, mainly from the wells outside the wellfield towards south, in order to check and confirm the conceptual model of the Mutnovsky reservoir;
2. A new long term group flow test in order to calibrate a numerical model of the Mutnovsky reservoir. During this new flow test, the downhole pressure in monitoring wells should be measured, while the production wells are flowing, in order to obtain pressure interference between wells; estimate reservoir permeability and estimate the field wide pressure response to production.

ACKNOWLEDGMENTS

I wish to express my hearty thanks to my advisors Mr. Grimur Bjornsson and Mr. Benedikt Steingrimsson for their valuable help in preparing this report and also for the lectures during the training programme. I would also wish to thank Helga Tulinius, Pordur Arason and Josef Holmjarn for their advice and useful suggestions. Special thanks to Dr. Ingvar B. Fridleifsson, director of the UNU Geothermal Training Programme, for his excellent guidance and successful operation of the programme. Ludvik S. Georgsson and Margret Westlund are thanked for their kind and useful care during the geothermal training in Iceland.

NOMENCLATURE

C_r	= Rock heat capacity (kJ/kg°C)
c_w	= Compressibility of water
c_r	= Compressibility of rock
E_s	= Stored heat in the geothermal system (kJ)
E_f	= Stored heat in the fluid (kJ)
E_r	= Stored heat in the rocks (kJ)
h	= Enthalpy of fluid (kJ/kg)
h_r	= Enthalpy of fluid at reference temperature (kJ/kg)
h_{s1}	= Enthalpy of steam at initial saturation conditions (kJ/kg)
h_{s2}	= Enthalpy of steam at final saturation conditions (kJ/kg)
h_{w2}	= Enthalpy of water at final saturation conditions (kJ/kg)
M	= Fluid mass withdrawn due to expansion (kg)
M_s	= Steam mass withdrawn due to boiling into the reservoir (kg)
m_f	= Thickness of permeable intervals in wells (m)
m_r	= Thickness of reservoir (m)
P_1	= Initial reservoir pressure (bar)
P_2	= Final saturation pressure (bar)
P_{min}	= Minimum reservoir pressure that allows discharge from wells (bar)
Q_e	= Heat yielded due to expansion (kJ)
Q_s	= Heat yielded due to boiling into the reservoir (kJ)
R_f	= Recovery factor
S	= Saturation of steam in the reservoir
T	= Temperature (°C)
T_r	= Reference temperature (°C)
V	= Reservoir volume (m ³)
α_r	= Coefficient of reservoir heat exchange efficiency
ρ_r	= Density of rock (kg/m ³)
ρ_f	= Density of fluid (kg/m ³)
ρ_w	= Density of water (kg/m ³)
ρ_{w1}	= Density of water at initial saturation pressure (kg/m ³)
ρ_{w2}	= Density of water at final saturation pressure (kg/m ³)
ρ_s	= Density of steam (kg/m ³)
ρ_{s2}	= Density of steam at final saturation pressure (kg/m ³)
ϕ	= Rock porosity

REFERENCES

- Arason, P., and Bjornsson, G., 1993: *ICEBOX. User's guide*. Orkustofnun, Reykjavik.
- Bjornsson, G., 1994: *Assessment of the geothermal reserves, Iceland*. UNU, Iceland, unpublished lecture notes.
- Bjornsson, G., and Bodvarsson, G., 1993: A multi-feedzone wellbore simulator. *Geoth. Res. Council, Trans. 11*, 503-507.
- Helgason, P., 1993: *Step by step guide to BERGHITI. User's guide*. Orkustofnun, Reykjavik.
- Kiryukhin, A.V., 1992: *Progress report on modelling studies: natural state conditions and exploitation of the Dachny geothermal reservoir, Mutnovsky hydrothermal system, Kamchatka, Russia*. Lawrence Berkeley Lab., Berkeley, report LBL-32729, 21 pp.

Kiryukhin, A.V., 1993: High-temperature flows in the Dachny field of the Mutnovsky hydrothermal system, Russia. *Geothermics*, 22, 49-64.

Perveev, S.L., Assaoulova, N.P., and Gunina, I.V., 1992: *The results of exploration works in the Mutnovsky geothermal field*. Internal report of the Kamchatka hydrogeological division (in Russian), 142 pp.

Sarmiento, Z., 1993: *Geothermal development in the Philippine*. UNU G.T.P., Iceland, report 2, 99 pp.

Vakin, E.A., Kirsanov, I.T., and Kirsanova, T.P., 1976: *The thermal grounds and the hot springs of the Mutnovsky volcanic region*. Eastern scientific centre, Vladivostok city, 85-114, (in Russian).

APPENDIX I: Temperature maps and cross-section from the Mutnovsky geothermal field

FIGURE 1: Location of boreholes, and temperature and pressure cross-sections in the Mutnovsky geothermal field

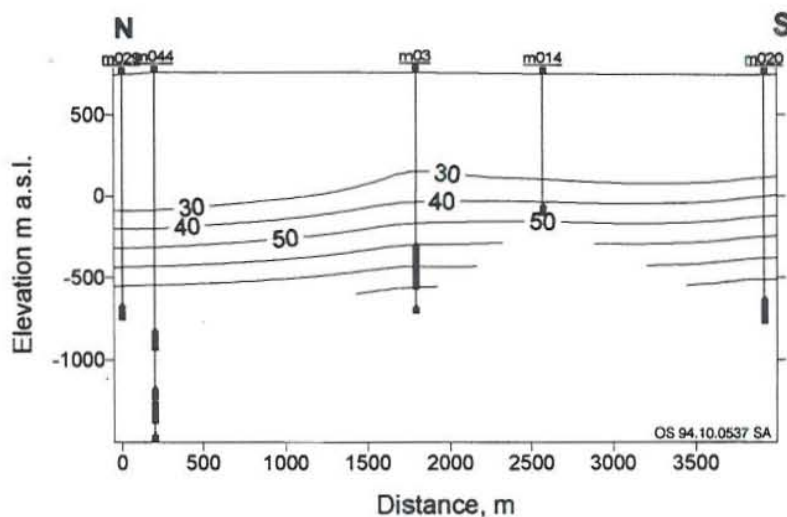
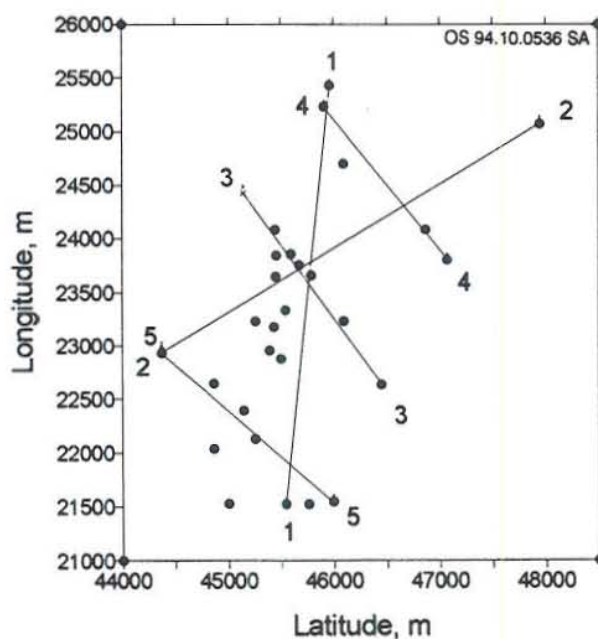


FIGURE 2: Pressure (bar-g) in cross-section 1-1, permeable parts of the wells are shown in bold

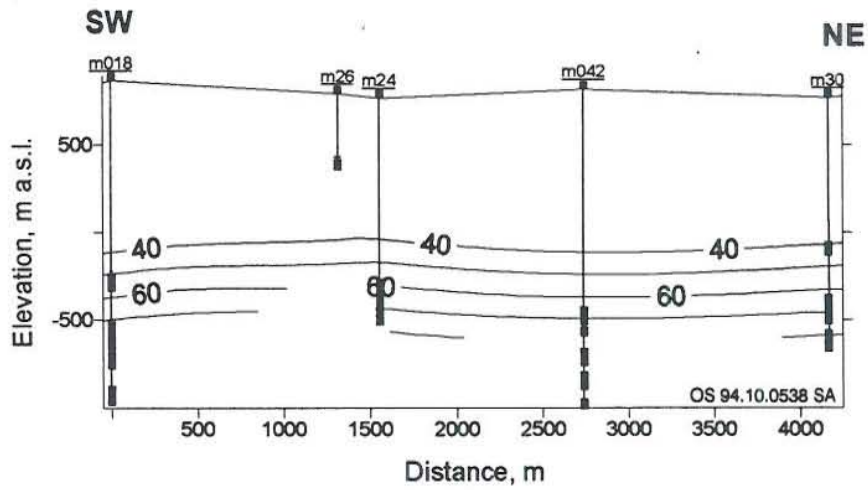


FIGURE 3: Pressure cross-section 2-2

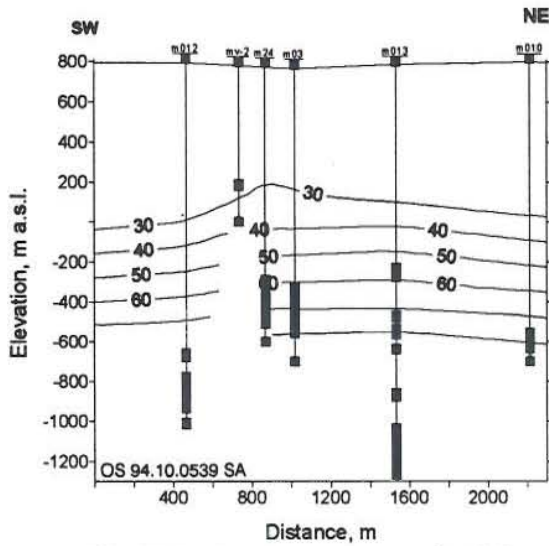


FIGURE 4: Pressure cross-section 3-3

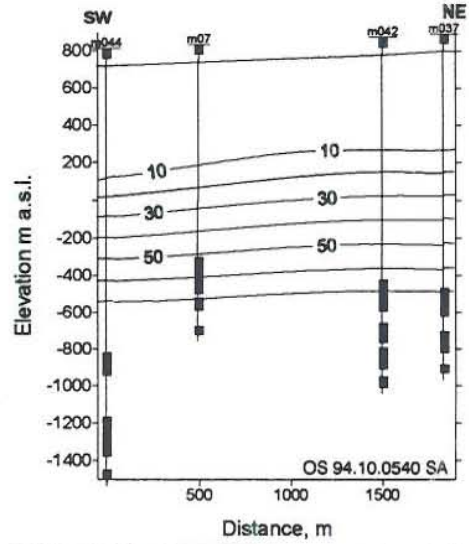


FIGURE 5: Pressure cross-section 4-4

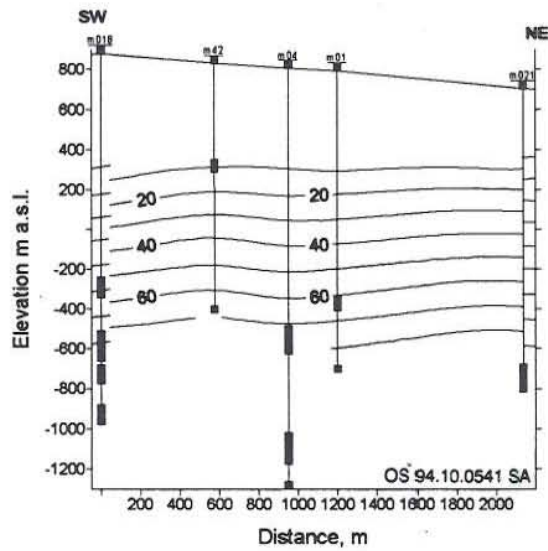


FIGURE 6: Pressure cross-section 5-5

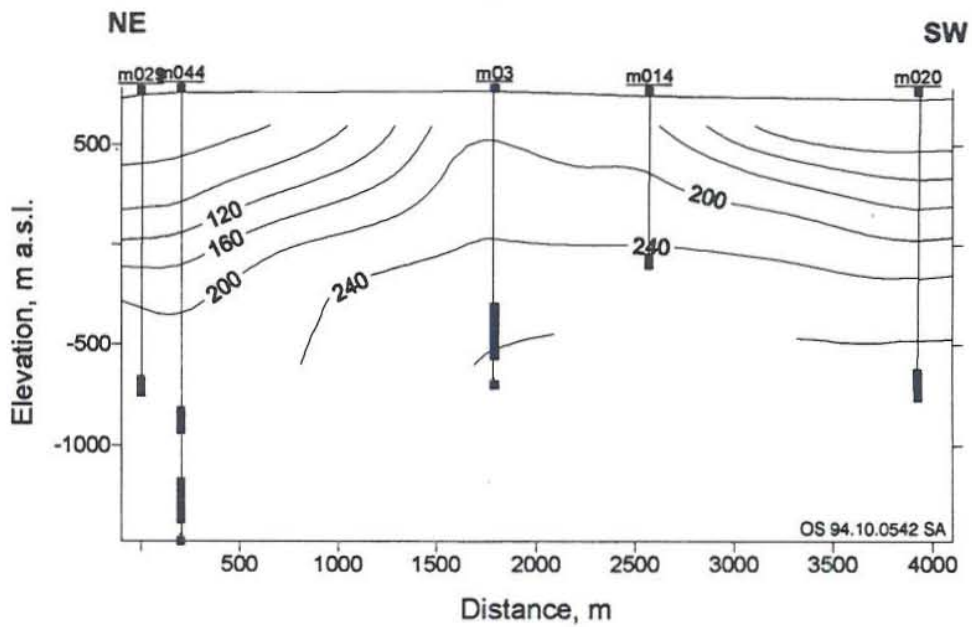


FIGURE 7: Temperature (°C) in cross-section 1-1, permeable parts of the wells are shown in bold

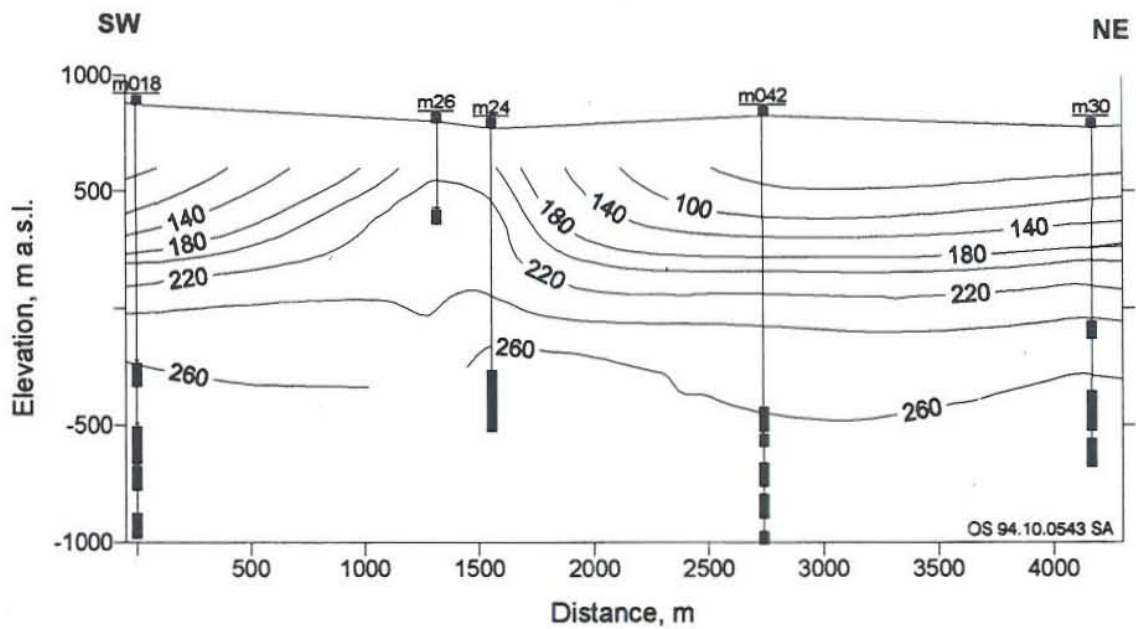


FIGURE 8: Temperature cross-section 2-2

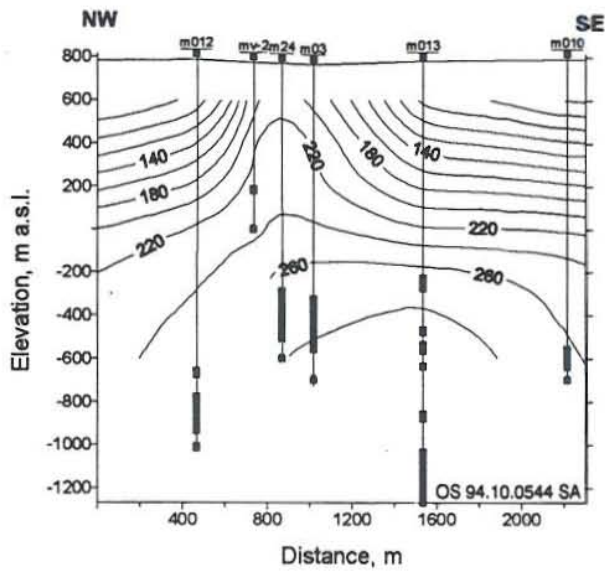


FIGURE 9: Temperature cross-section 3-3

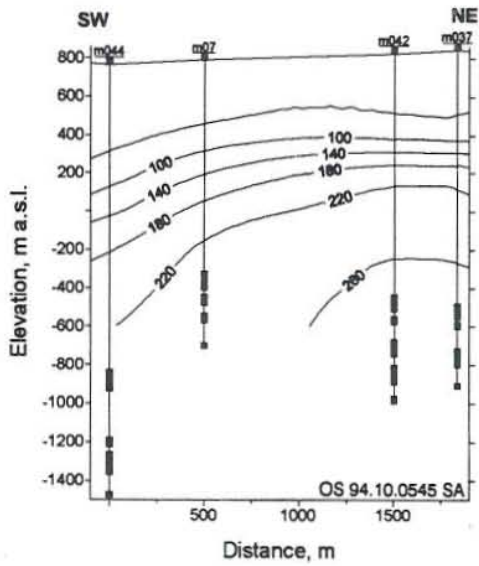


FIGURE 10: Temperature cross-section 4-4

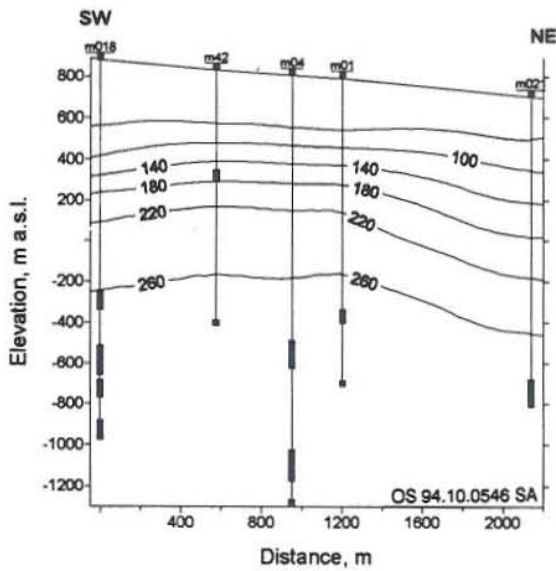


FIGURE 11: Temperature cross-section 5-5

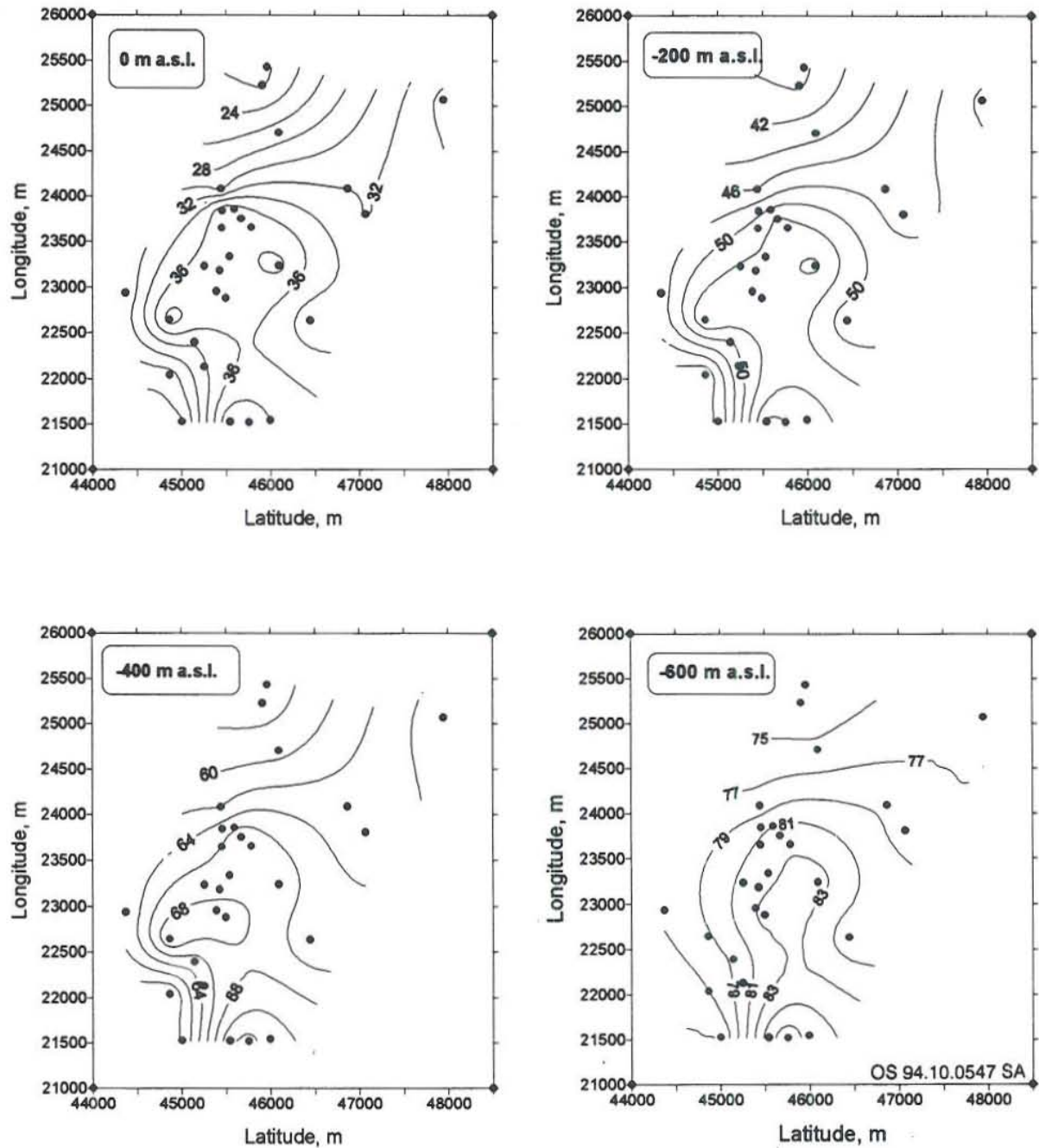


FIGURE 12: Pressure distribution maps (bar-g) in the Mutnovsky field at selected elevations

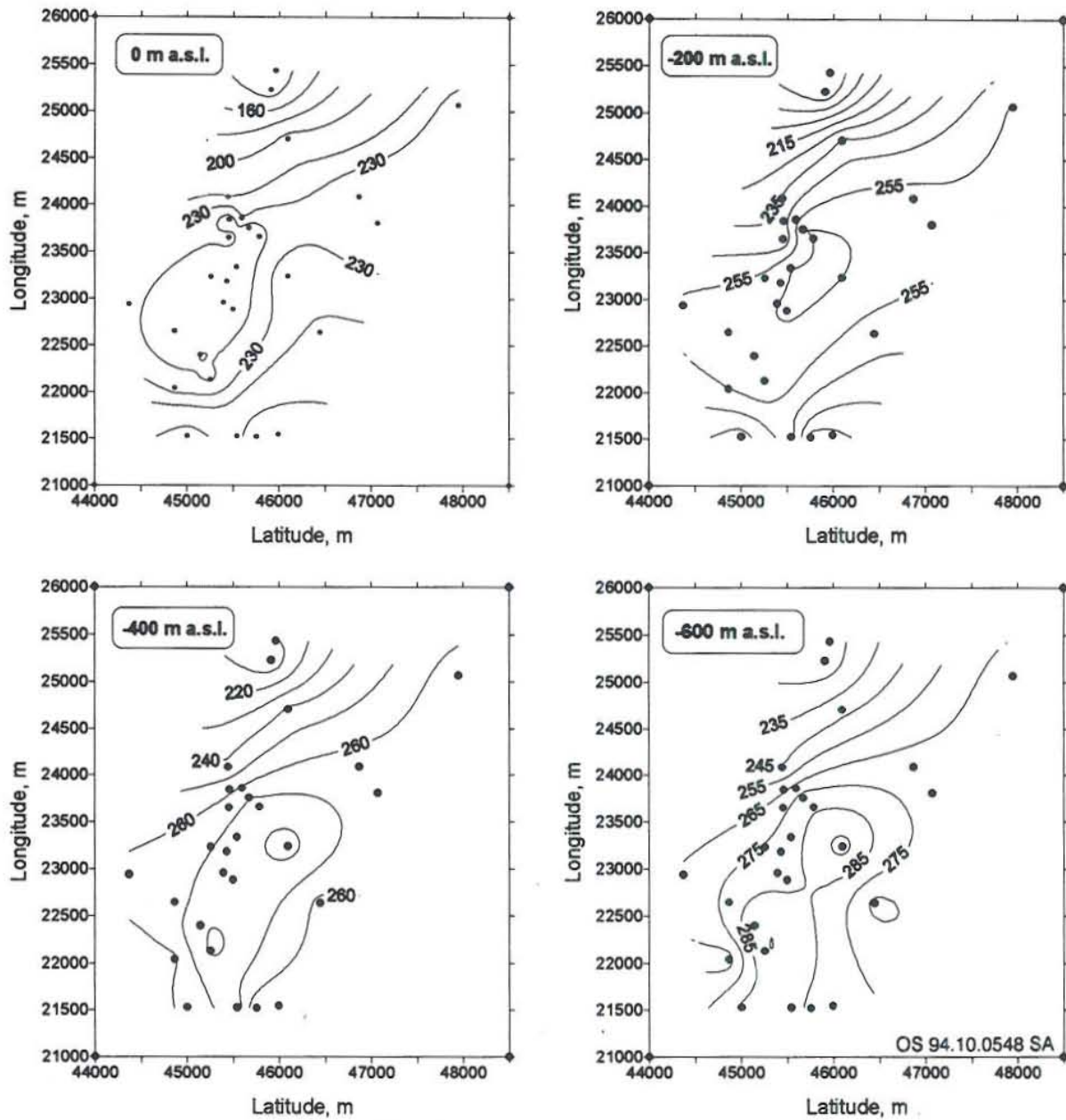


FIGURE 13: Temperature distribution maps (°C) in the Mutnovsky field at selected elevations